HYDROGELS AND SELF-ASSEMBLED NANOSTRUCTURES BASED ON WOOL KERATOSE

A Thesis Submitted to
the Graduate School of Engineering and Science of
İzmir Institute of Technology
in Partial Fulfillment of the Requirements for the Degree of

MASTER OF SCIENCE

in Chemical Engineering

by
Efecan PAKKANER

July 2017
İZMİR

We approve the thesis of **Efecan PAKKANER**

Examining Committee Members:

Assist. Prof. Dr. Ayben TOP
Department of Chemical Engineering, İzmir Institute of Technology

Prof. Dr. Muhsin ÇİFTÇİOĞLU
Department of Chemical Engineering, İzmir Institute of Technology

Assist. Prof. Dr. Çisem BULUT ALBAYRAK
Department of Food Engineering, Adnan Menderes University

14 July 2017

Assist. Prof. Dr. Ayben TOP
Supervisor, Department of Chemical Engineering, İzmir Institute of Technology

Prof. Dr. Fehime ÇAKICIOĞLU ÖZKAN
Head of the Department of Chemical Engineering

Prof. Dr. Aysun SOFUOĞLU
Dean of the Graduate School of Engineering and Sciences

ACKNOWLEDGEMENTS

On the way of conducting this research and writing the thesis, there are several people that have influenced me whom I would like to mention about that I am thankful for. Without them, I would never have been able to execute this dissertation by any means.

Firstly, I would like to express my most sincere thankfulness to my supervisor Assist. Prof. Ayben Top. From the very first day that I have been in her laboratory, the dynamism, passion and the thrive for exploring that she possessed pushed up the envelope for me; and thanks to her remarkable supervising, kindness, patience and extensive knowledge, I have come a long way. Her strong presence in the laboratory has also made things considerably easier for me, as I have had the chance to benefit from her experiences at first hand and that made me grasp much more than I have ever expected.

I would also like to thank to my committee members, Assist. Prof. Dr. Çisem BULUT ALBAYRAK and Prof. Dr. Muhsin ÇİFTÇİOĞLU for their patience and kindness, as well as their navigation to enrich the context of the study. Prof. Dr. Muhsin ÇİFTÇİOĞLU was also thanked for letting me to access the rheometer, making me possible to conduct the rheological studies.

Specifically, I would like to thank my dear friends Okan Akın, Özgün Deliismail, Bertan Özdoğru, Aydın Cihanoğlu, Kaan Yaltrık, Ceren Kımna, Elif Güngörmüş, Alaz İzer, and many more that I am unable to mention at the moment; for their support and kind friendship throughout the period that I have been here. I would also like to thank some old friends, lab members and staff, including Damla Yalçın, Berk Uysal, Nesligül Yüksel, Beste Balcı, Hayrullah Çetinkaya, Çağla Gündoğan, Önder Tekinalp, Ahmet Kurul, Ahmet Köken, Nazil Karaca, Belgin Tuncel, Burcu Alp, Deniz Şimşek and Özlem Çağlar Duvarcı, that somehow have had significance on me in my journey.

To the ones that have always been with me, both physically, mentally and spiritually; from the bottom of my heart, I wish to warmly thank my mother and father; for their endless love, and indestructible support on wherever I have headed for and whatever I have intended to do. Without their sacrifice and devotion, I would never able to be the person that I am today. They are the honorary authors of this thesis.

Last but most definitely not the least, I, with deepest pleasure, would like to thank in the dearest way to my girlfriend, Gülce Kalyoncu, for being there, for me, from the first day that we have met in Ege University up to this very precious moment that I am

writing these lines to express my deepest gratitude for her. The smart thoughts that came from her beautiful mind and the never-ending encouragement brewed from her generous spirit, combined with a heavenly smile and a heartwarming laughter, made me carry on and never be discouraged; no matter what obstacle I have encountered on the way. Thank you, my dear.

ABSTRACT

HYDROGELS AND SELF-ASSEMBLED NANOSTRUCTURES BASED ON WOOL KERATOSE

In this study, water soluble keratose proteins were extracted from "*Ovis aries*" wool using peracetic acid oxidation with a yield of 35 ± 5 %. Wool samples and the extracted keratose proteins were characterized by using FT-IR, XRD, SEM and TGA techniques. α-keratose fractions (MW = 43-53 kDa) along with cleaved fragments of α-keratoses with molecular weights between 23 and 33 kDa were identified in the extracted protein mixture using SDS-PAGE analysis. DLS and AFM experiments indicated self-assembled globular nanoparticles with diameters of ~20-40 nm formed at 5 and 10 mg/ml keratose concentrations. On the other hand, at 10 % w/v keratose concentration interconnected keratose hydrogels with pore sizes of 6 ± 4 and 7 ± 4 μm were obtained upon incubation at 37 and 50 °C, respectively. Storage moduli (G') of these physical hydrogels were increased from ~100 to ~1000 Pa, as gelation temperature was increased from 37 to 50 °C. Hydrogels were also obtained at 7.5 % w/v keratose concentration by the addition of a crosslinker, THPC. Amine group:crosslinker ratio was used as 1:1, 1:2 and 1:4. As the amount of crosslinker increased, network transformed from fibrous to more planar structures exhibiting a significant decrease in average pore size from 24 to 11 μm. G' values of the crosslinked hydrogels were obtained between ~1 and ~5 kPa tuned by the crosslinking amount. Cell interaction properties of a select physical hydrogel prepared at 37 °C was tested using CCK-8 assay. It was observed that the keratose hydrogel supported L929 mouse fibroblast cell proliferation as much as collagen, which suggests that these keratose hydrogels can be promising candidates in soft tissue engineering applications.

Keywords and Phrases: Self-assembly, keratose, hydrogels, biomaterials, nanostructures, wool keratin based materials

ÖZET

YÜN KERATOZU BAZLI HİDROJELLER VE KENDİLİĞİNDEN DÜZENLENEBİLEN NANOYAPILAR

Bu çalışmada, keratoz proteinleri, *"Ovis aries"* adı verilen evcil koyun türünün yününden, perasetik asit oksidasyonu kullanılarak yaklaşık 35% verim ile çıkartılmıştır. Yünler ve elde edilen keratoz proteinleri, FT-IR, XRD, SEM ve TGA teknikleri ile karakterize edilmiştir. SDS-PAGE analizi ile bu protein karışımının 43-53 kDa molekül ağırlığına sahip olan α-keratoz proteinlerinden ve 23-33 kDa aralığında bu proteinlerin parçalarından oluştuğu saptanmıştır. DLS ve AFM testleri, 5 ve 10 mg/ml derişime sahip keratoz çözeltilerinin 20-40 nm hidrodinamik çapa sahip küresel nanotaneciklere kendiliğinden düzenlendiğini göstermiştir. Öte yandan, keratoz konsantrasyonu 100 mg/ml seviyesine çıkarıldığında ve sırasıyla 37 ve 50 °C sıcaklıklar altında inkübe edildiğinde, ortalama gözenek boyutları sırasıyla 6 ± 4 and 7 ± 4 μm olan hidrojel ağlarının elde edildiği görülmüştür. Bu fiziksel hidrojellerin inkübasyon sıcaklıklarının 37 °C'den 50 °C ye çıkarılmasıyla, saklanan modül (G') değerinin 100 Pa'dan 1000 Pa değerine çıktığı gözlemlenmiştir. Hidrojeller ayrıca kütlece % 7.5 keratoz konsantrasyonuna sahip olan protein çözeltilerine THPC kimyasal çapraz bağlama ajanları eklenerek de oluşturulmuştur. 1:1, 1:2 ve 1:4 amin grubu:çapraz bağlayıcı oranlarında 3 farklı tipte kimyasal hidrojel hazırlanmıştır. Bu oran arttıkça, jel ağının iğsi yapıdan düzlemsel yapıya doğru değiştiği ve ortalama gözenek çapının 24 μm'den 11 μm'ye düştüğü gözlemlenmiştir. 1 kPa ve 5 kPa arasında elde edilen G' değerlerinin THPC miktarının değişimi ile kontrol edilebildiği saptanmıştır. 37 °C'de hazırlanmış seçilmiş fiziksel hidrojelin hücre etkileşim özellikleri CCK-8 yöntemi ile test edilmiştir. Bu hidrojelin L929 fare fibroblast hücrelerinin büyümesini kollajen kadar desteklediği görülmüş ve keratoz bazlı hidrojellerin yumuşak doku mühendisliğinde gelecek vaat eden adaylar olabileceği öngörülmüştür.

Anahtar Kelimeler ve Deyimler: Kendiliğinden düzenlenme, keratoz, hidrojeller, biyomalzemeler, nano yapılar, yün keratini bazlı malzemeler

TABLE OF CONTENTS

LIST OF FIGURES

Figure **Page**

LIST OF TABLES

Table **Page**

NOMENCLATURE

Abbreviations

AFM	Atomic Force Microscopy
DLS	Dynamic Light Scattering
FT-IR	Fourier Transform Infrared
PBS	Phosphate Buffer Saline
SDS-PAGE	Sodium Dodecyl Sulfate Poly Acrylamide Gel Electrophoresis
SEM	Scanning Electron Microscopy
TGA	Thermogravimetric Analysis
THPC	Tetrakis (hydroxymethyl) Phosphonium Chloride
XRD	X-Ray Diffraction

CHAPTER 1

INTRODUCTION

Self-assembly of molecules from biological origin to form nano-complex structures has been a popular research trend throughout the years due to successful adaptations of this 'bottom-up' approach to innovative biological and medical applications and other various technologies [1,2]. Briefly, spontaneous association of these molecules creates supramolecular architectures that are thermodynamically and mechanically stable at desired conditions with the possibility of precise control of construction via changing the physical parameters, including temperature, pH, ionic strength, light intensity, electric and magnetic fields [1,3,4]. Driven by non-covalent forces such as hydrogen bonding, hydrophobic attractions, van der Waals and electrostatic interactions, self-assembly of proteins and peptides facilitated the formation of a variety of nanostructures including nanofibers, nanorods, nanotubes and nanoparticles [2,5-13]. Although numerous synthetic and natural polymers can undergo self-assembly process, polymers from natural origin have gained a wider attraction as biomaterials due to their high bio-compatibility and significantly low cytotoxicity, as well as bio-inertness and bio-molecular recognition abilities [14,15].

Keratin can be extracted from various body parts of birds, reptiles and mammalian species, including hair, wool, nails, horns, hooves and feathers. Thus, being the major by-product of the well-grown industries such as breeding, textile, wool and butchery, keratin is one of the most abundant biopolymers [16,17]. Different from the other proteins, it contains quite high cysteine content (7-20%) that promotes its mechanical, chemical and thermal stability properties by the aid of the disulfide bonds present in their structures [18,19]. Like the other biopolymers from biological origins such as collagen, elastin and chitosan, keratin alone and mixed with other polymers have been tested in various biomedical applications such as delivery of bioactive agents [20-22], wound healing [16,23-25], and bone tissue engineering [26-28]. It has been almost genuinely proven that keratins are promising candidates as sustainable biomaterials due to their abundance, easy handling, affordability and biocompatibility.

Among the available sources of keratin, wool keratins have received more interest than the keratins from the other body parts such as horn and hoof due to their abundance, higher extraction yields and structural advantages such as hygroscopicity. Additionally, it was reported that wool keratin has cell attachment units such as arginine-glycine-aspartic acid (RGD) and leucine-aspartic acid-valine (LDV) groups in its aminoacid sequence, which can be found in many extracellular matrix proteins like fibronectin [29,30]. Unsurprisingly, wool keratin film provided better attachment platform for fibroblasts compared to collagen film [31], and wool keratin derived sponges have been demonstrated to be suitable for long-term cell cultivation [29].

Although biomaterials based on keratins have been shown to be quite promising, one major concern that limits their application spectrum can be their poor solubility in aqueous medium due to the disulfide bridges that form easily by simple air oxidation of extracted keratin proteins. One of the methods to obtain soluble proteins from keratins is oxidative extraction which gives keratoses via breaking of disulfide bonds and converting thiol groups of cysteines to sulfonic acid. Recently, keratoses from human hair [32], and Merino wool [30] have been reported to form hydrogels at high concentrations. In this study, wool from Akkaraman sheep breed was used as a keratose source. Structural and thermal characterization of wool and keratose were performed. Size, morphology and conformation of self-assembled nanostructures of keratose obtained at low concentration regime were investigated. Physically and chemically crosslinked hydrogels were prepared at high keratose concentration and conformational, morphological, rheological and in vitro cell proliferation properties of the hydrogels were evaluated.

In the following literature review section (Chapter 2), hydrogels and self-assembled nanostructures based on biopolymers were briefly explained. Keratin structure and extraction procedures were explained and select studies related to the use of keratin in various biomedical applications, such as tissue engineering, drug delivery and/or wound healing were provided.

Chapter 3 includes experimental methods used in this study. Details of extraction procedure of keratose, preparation of nanostructures, self-assembled and crosslinked hydrogels along with the characterization techniques used were given.

In Chapter 4, structural, thermal, and morphological characterization results of wool samples were discussed. Conformational and morphological properties of keratose at different concentrations were presented. Rheological properties of the physical hydrogels prepared at different temperatures and chemical hydrogels prepared at different

crosslinker amounts were investigated. Finally, as a preliminary study, interactions of a select hydrogel system were evaluated using cell proliferation and live/dead assay.

Finally, in Chapter 5, conclusions of the study were presented along with the proposed continuation experiments. Future prospects of the keratose based nanostructures and hydrogels were discussed.

CHAPTER 2

LITERATURE SURVEY

This chapter presents a brief literature survey about hydrogels, keratin based materials; the recovery methods of soluble keratins and their effects on the properties of the resulting biomaterials, the studies that focus on the compatibility of keratin based materials on different cell lines and/or tissues as well as with the studies that are based on comparable properties of hydrogels including mechanical strength, crosslink density and self-assembly behaviors.

2.1. Hydrogels

Hydrogels are consisted of 3-D complex hydrophilic network structures and can retain large amounts of water or biological fluids [33]. They can be produced using a wide range of natural and/or synthetic materials including natural and/or synthetic polymers, carbohydrates, natural gums, polyacrylates, polysaccharides, peptides and proteins [34]. In addition to that remarkably wide selection of base materials, their structural integrities could easily be conducted by crosslinking reactions, that could be associated by both physical and chemical treatment. Moreover, they are often stated as excellent sub-groups of biomaterials, due to their tissue mimicking abilities, tunable properties, biocompatibility and biodegradability functions. Also, the formulation of hydrogels can be achieved at various forms and structural shapes including nanoparticles, coatings and films, which consequently makes them favorable and superior to use in many biomedical applications with ease [35,36].

Their high potential of swelling is a huge plus on their side, however their hydrophilic abilities are often specified with the presence of some specific side groups, including –COOH, –OH, $–CONH_2$, –CONH–, and $–SO_3H$ as their network side chains.

Hydrogels can be classified with respect to several sub-groups, as seen below [37].

- **Source:**
  - Natural hydrogels
  - Hybrid hydrogels
  - Synthetic hydrogels
- **Crosslinking:**
  - Physically crosslinked hydrogel
  - Chemically crosslinked hydrogel
- **Ionic charge:**
  - Non-ionic hydrogels
  - Ionic hydrogels
  - Cationic hydrogels
  - Ampholytic hydrogel
- **Preparation method:**
  - Homo-polymers
  - Copolymers
  - Interpenetrated polymers
- **Biodegradability:**
  - Biodegradable hydrogels
  - Non-biodegradable hydrogels
- **Physical Properties:**
  - Smart hydrogels
  - Conventional hydrogels

In terms of the way they are fabricated, the type of crosslinking has distinctive influence on the resulting hydrogel and its chemical properties. If a hydrogel is crosslinked with the help of an external chemical agent, it is called a chemically crosslinked (or a "permanent") hydrogel. The three-dimensional complex network is held together by covalent forces, and unless those covalent bonds are broken, they do not dissolve in solvents. That primary covalent bonding in the structure gives the hydrogels mechanical stability and high order of swelling and these properties can be tuned with the degree of crosslinking. As a negative aspect, chemically crosslinked hydrogels may release highly toxic chemicals whilst forming, and prior to using as a biomaterial, an effective discharge of these toxic materials must be done [37]. Also, the homogeneity of the chemical hydrogels would not be well established, since the hydrophobicity of the crosslinking agent can yield to unwanted aggregations, often called as the "clusters". Moreover, the structural integrity of the material could not be controlled easily when tried to be injected, and the equilibrium swelling -which depends on the crosslinking density- could change spatially, because of the presence of undesired voids or macropores [38]. Physical hydrogels on the other hand, (also called as "reversible" hydrogels) do not need an external crosslinking agent to be produced. They are formed and stabilized by highly ordered molecular aggregates which have been associated by secondary forces such as

van der Waals forces, hydrophobic interactions and hydrogen bonding that are formed within the structure that are mostly consisted of reversible interception domains. Different from the chemical gels, their equilibrium swelling behaviors can be influenced by external parameters called as “physical stimuli” (e.g. temperature, pH, ionic strength, irradiation, etc.). However, the point they are inferior to the chemical hydrogels is that, they will dissolve in water or another solvent, and they may show lower heat resistance when compared to chemical hydrogels.

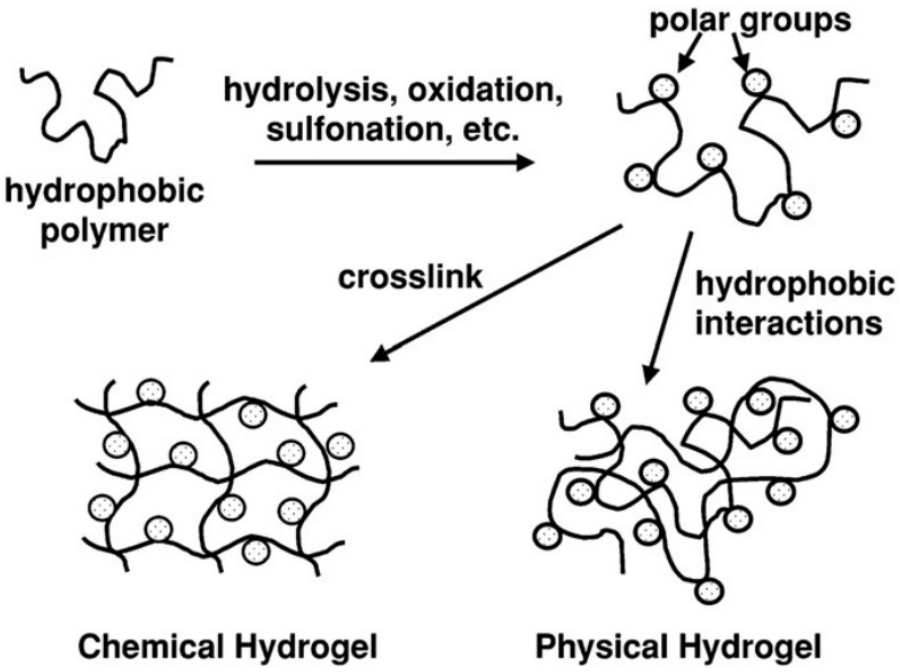

Figure 2.1. Schematic Representation of physical and chemical hydrogel preparation (Source: [38])

As their advantages are globally well-documented, hydrogels are popular biomaterials offered in a wide range of biomedical and pharmaceutical applications, including tissue engineering, drug and gene delivery, bio-sensing, wound healing, sutures, bio-adhesives, bio-sealants [39]. As the context of the current chapter, recent studies that are focused on the latest advancements happening in those mentioned applications were given.

2.2. Biomaterial Applications and Self-Assembly of Biopolymers

Among the wide-range of materials that could be used for producing hydrogels, biopolymers are rather preferable, especially to be used in biomedical and pharmaceutical applications due to their decent biocompatibility and biodegradability properties [40]. Numerous studies that were conducted that focus on natural and synthetic polymers, from a biomaterial and nanotechnology perspective. Sionkowska has prepared an extensive review about both natural polymers and their blends with synthetic polymers to be used as biomaterials, as well as with the recent technologies used in their development stages [40]. She has discussed the biomaterial properties of various natural polymers including chitosan, collagen, elastin and keratin. She further expanded the review by pointing out the studies that focus on the blends of these natural and synthetic polymers including PVA, PEO, along with their possible uses in biomedical applications. Although she has obtained the promising results which support that natural polymers can be used as biomaterials, she has noted that there should still be some long way to go for them to be commercialized. As another biopolymer based study, Silva and his colleagues have explained the process of developing protein-based biomaterials, and stating the possible advantages of using proteins in biomaterial development, predicating some benefits including their outstanding biocompatibility and biodegradability [41]. They have specified various types of proteins, by expressing their chemical compositions, molecular conformations and how they can be extracted and/or produced from natural sources such as silk and keratin. Additionally, they have presented numerous examples from recent applications and variations from studies on how protein based materials show remarkable cell and tissue interaction. To give just a few examples, they have stated that keratin nanofibers could be strong candidates for biomaterials such as scaffolds, sponges and fibrous membranes to be used in cell and tissue engineering applications when blended with both natural and synthetic polymers. There is a vast number of studies that have been carried out by blending biopolymers, and the cell interactions were monitored. Wang et al. have prepared keratin based nanofibers that are supported with PVA, and their results have shown a decent biocompatibility and cytotoxicity on dorsal tissues of a specific rat species [25]. Moreover, Li et al. have developed mats that are blends of poly-caprolactone and keratin fibers, in order to be used as scaffolds for vascular tissue engineering [42]. They have claimed that, the scaffolds which were supported with synthetic polymers had

better cytotoxicities when compared with the ones that only contain ε-caprolactone with mouse fibroblast cells, and they could find a large portion of usage area to be used as scaffolds.

Self-assembly of nanomaterials into more complex hierarchical structures have always been an attractive area of interest, especially for biomaterials since materials that assembled from biopolymers have some powerful advantages, including less chemical agent influence and homogeneity on the overall architecture. To support that hypothesis, Devine and Higginbotham have pointed out the main differences of chemically and physically prepared PVA polymeric gels in terms of mechanical strength and constructional homogeneity. They have implemented that physically prepared gels have possessed better mechanical properties in the short term, because of the crystalline architecture that can provide a more distributed load bearing [43]. As a common way to prepare biomaterials, the self-assembly behavior has been tested many times with biopolymers. When assembling, it is really important to note that secondary conformation of the structures (especially on peptide & protein based biomaterials) has a huge influence on the process. On one hand for peptides, a comprehensive review has been written by Pugliese and Gelain, that comprises self-assembly mechanisms and resulting biomaterial products [2]. On proteins on the other hand, Vu and her co-workers have prepared silk and wool keratin based biomaterials in different concentrations that are able to self-assemble into hydrogels. They have stated the importance of secondary conformation of the proteins on the action of self-assembling; as β-sheet crystals had been highly decisive on the formation of resulting hydrogel structure [33].

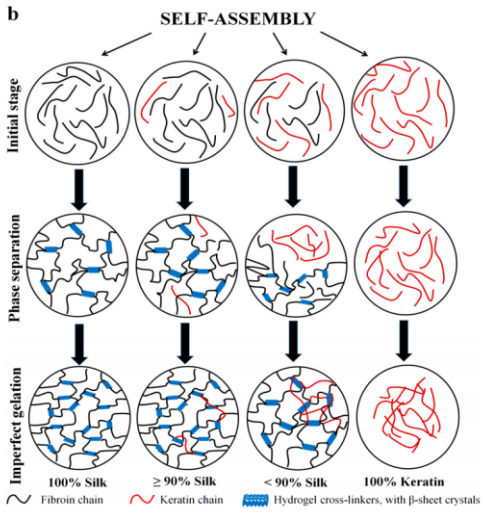

Figure 2.2. Self-assembly mechanisms of silk, keratin and silk-keratin blend fibers (Source: [33])

2.3. Keratin

Being the major by-product of the well-grown industries such as breeding, textile, wool and butchery; keratin possesses a tremendous amount of potential of recovery in order to be used as nano-fibrous biomaterials, considering the vast amount of waste produced all around the world [33,44]. They are one of the most abundant biopolymers known in nature, and together with collagen, are thought to be the most important biopolymers in animal species [45]. Among the 19 natural amino acid residues that it is composed of, what makes keratin differ from the other siblings of the protein family is the plethora of the cysteine residues present in its form (around 7-20% in total) [18], that gives the material mechanical, chemical and thermal stability features by the aid of the disulfide bonds present in their structures [19]. There exist numerous potential body parts for the extraction process from various species such as birds, reptiles and mammalians; including hair, wool, nails, horns, hooves, feathers and many more. Although there is a wide range of selection for the sake of potential sources, the properties of the extracted keratins vary from species to species, also from body part to part. There are three types of keratins discovered α, β and γ keratins [41,45]. The first group, α-keratins, are located in the center of the fiber cortex of the body part that they belong to, typically having an average molecular mass of 40 to 68 kDa. They can self-assemble into long and strong fibers that are called Keratin Intermediate Filaments (KIF), with a secondary structure of α-helix [46]. They are mostly poor in cysteine residues (different from the β-keratins) and majority of this type of keratins are found in mammal species (Table 2.1.). β-keratins on the other hand, are rather difficult to extract because of the β-sheet crystalline structures they possess, supported by the intermolecular hydrogen bonds, and their primary objective is to cover the cortical filaments and exhibit a protection from physical and chemical impacts. Their average molecular weights are measured to be 10-22 kDa, which is considerably lower than the α-keratin filaments [41]. Finally, γ-keratins that are considered as a sub-group of the α-keratins, and they are thought to have adhesive properties that holds the α-keratin filaments together, and consisted of globular compounds, with an average molecular weight of 15 kDa. Among the sources mentioned, wool has been extensively studied as an exemplary structure of α-keratins, along with feathers which are considered as the representatives of β-keratins.

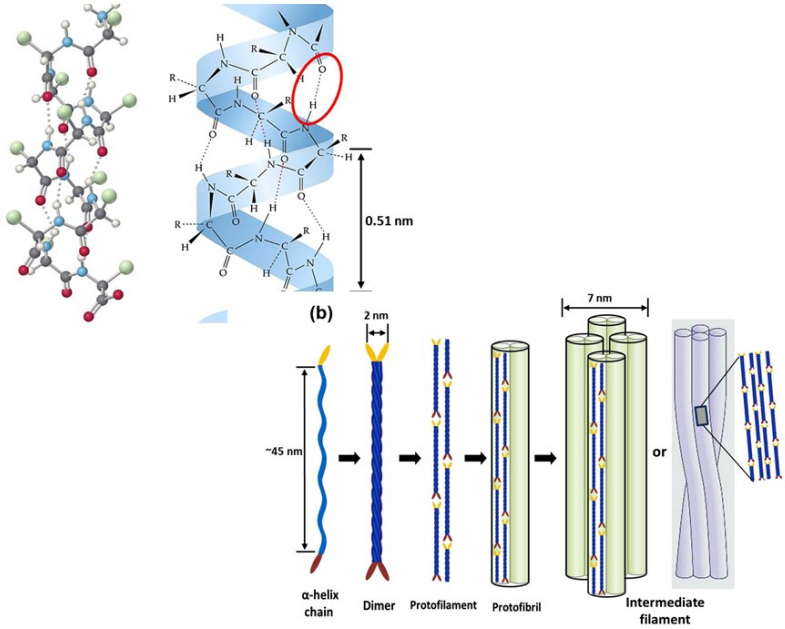

Figure 2.3. Intermediate filament formation and secondary structure of α-keratins (Source: [45])

In the case of α-keratins (Figure 2.3), which are known to be rich in α-helical content, that gives them the ability to form long and strong filaments [46], there are several interesting studies where it is claimed that the helical compositions of the proteins could be predicted via mathematical models [47,48]. Moreover, the change in the secondary structure on the characteristics of the keratin based biomaterials have been reported several times; as in the work of Rouse and van Dyke it was revealed that the change in the secondary structure of keratin films from coiled coil to β-sheet has boosted its antithrombogenicity and cytocompatibility properties, with the addition of several more exemplary cases that have been given in the same work [49].

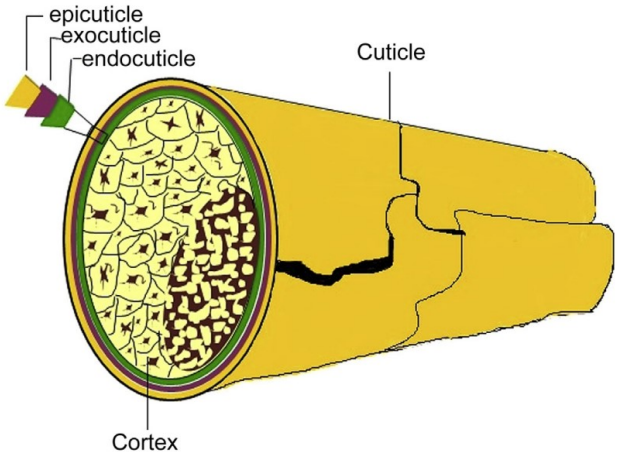

Figure 2.4. Schematic representation of a α-keratin fiber (Source: [46])

Table 2.1. Classification of the keratin types and the corresponding body parts they are found in (Source: [45])

Type of keratin	**Body Parts**
α-Keratin	Wool, hair, quills, fingernails, horns, hooves; stratum corneum
β-Keratin	Feathers, avian beaks and claws, reptilian claws and scales
α- and β-Keratin together	Reptilian epidermis, pangolin scales

Wool is a fiber structure which can be obtained from various mammalians such as sheep and certain other animals as was stated earlier. Composed of nearly 82% of keratinous protein substances [45,50], and the rest portion is called as the "non-keratinous" material, which is located in the Cell Membrane Complex (CMC). A single wool fiber is composed of main three parts; cuticle, cortex and medulla. A cross sectional representation of a wool fiber can be seen in Figure 2.5.

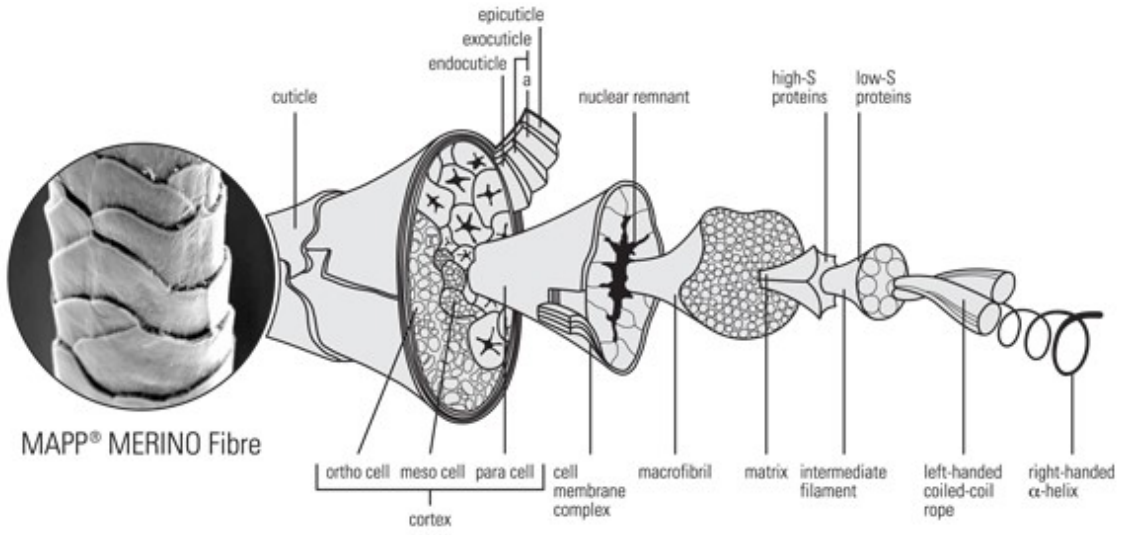

Figure 2.5. Cross-sectional representation of a merino wool fiber (Source: [51])

It has been well-documented that wool-derived keratins are biodegradable in the presence of trypsin, and its strong cell interaction and attachment abilities have been exhibited in numerous studies; including peripheral nerve cells [32], hepatocytes [52],

mesenchymal stem cells [53], fibroblasts and osteoblasts [18], where the attachment and the growth of the specific cell lines are supported by keratin mediated platforms. Moreover, keratin based biomaterials have been tested in various biomedical applications; such as drug delivery [22], wound healing [16,24], and tissue engineering as scaffolds [42,54], where it is almost genuinely proven that keratins are bright candidates to be used for biomedical purposes, thanks to their abundance, easy handling, affordability, biocompatibility and biodegradability, along with the presence of cell-binding peptide domains such as LDV (leucine-aspartic acid-valine) and RGD (arginine-glycine-aspartic acid) in their amino-acid sequences. Among the other sources of keratin, due to their higher extraction yields and structural advantages such as hygroscopicity, wool keratins step up further than the other body parts such as horn and hoof, the use of wool keratins seem more advantageous, yet the researchers have set their focuses on using regenerated keratins in order to prepare biomaterials.

Although the use of keratins for the manufacturing of biomaterials seems quite reasonable, due to the obvious advantages that have been mentioned above; one major obstacle to overcome is their poor solubility in the aqueous medium. For this purpose, several different approaches are present in the literature, which ends up with varying products that have different chemical and structural properties. While β-keratins can also be used to obtain solubilized keratin derived materials, use of α-keratins will be explained here, by explaining the chemical procedures and materials used for the corresponding processes. For α-keratins, solubility can be achieved by two major procedures; oxidation and reduction [55]. Among these two strategies, reduction yields a transformation of disulfide bonds into thiol groups (-SH), which have the potential of re-oxidizing to form the disulfide bonds and should be blocked (Figure 2.6). The resulting material is called as “kerateine” which is a less soluble and less hygroscopic fraction of a keratin, that still has the potential to form disulfide bonds in the presence of suitable conditions [56]. However, the oxidative process requires a chemical treatment is proposed to break the disulfide bonds and oxidizing the sulfur in the cysteine residues to sulfonic acids, which does not have the ability to form disulfide cross-links [57]. This derived material is often called as “keratose”, that is known as the soluble, oxidized form of keratins which is a hygroscopic protein and tend to degrade faster.

Moreover, recent studies have revealed that, these solubilized forms of keratins, or often referred as the Keratin Associated Proteins (or KAPs) [52] have shown to have a potential to self-associate or, in other words, self-assembly to more hierarchically complex structures such as gels [30].

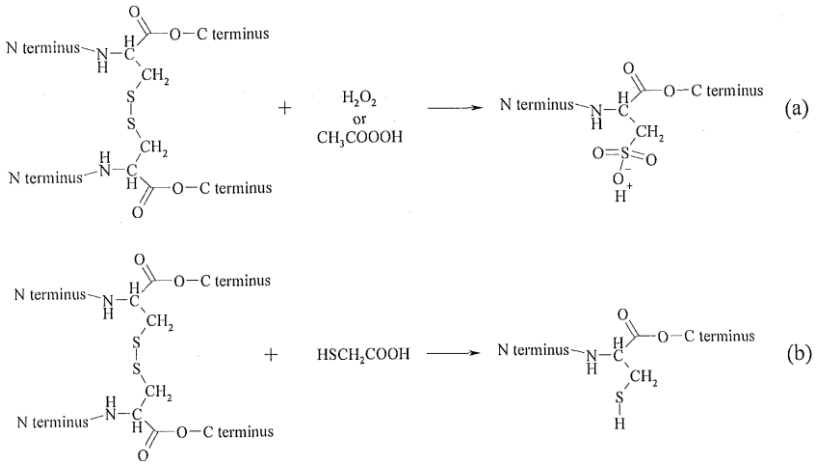

Figure 2.6. Formation of keratin derived materials via a) oxidation, b) reduction (Source: [58])

2.4. Keratin Based Biomaterials

The microstructural differences between keratoses and kerateines have major influence on how and when they could be used; since the hydrogels that are produced from keratoses are known to undergo a faster erosion process due to the lack of covalent bonding present in their structures -unless they are covalently crosslinked-. On the other hand, gels produced from kerateines have exhibited slower erosion characteristics, due to their ability to re-associate disulfide linkages. Giving that information, Ham et al., have attempted to get the best of two worlds; by preparing tunable hydrogels that could be used for the release of a specific growth factor. They have produced kerateine and keratose hydrogels individually, also blended them in different concentrations to get different hydrogel properties by self-assembly that was triggered thermally (by incubating at 37 °C overnight) [55]. As the kerateine concentration of the hydrogel mixture was increased, G' (strorage modulus) of the hydrogels increased as well. However, as keratose hydrogels were known to erode faster than the kerateine rich ones; the percent growth factor releasing amounts of keratose hydrogels have seemed to be larger than the other samples, reaching up to 70% release by the end of a 7-day period. The authors have also claimed

that by altering the hydrogel compositions, the nature of erosion could be tuned, as supported by the growth kinetics. Other than self-assembly, Sando et al., have prepared keratose hydrogels by crosslinking them with di-Tyrosine bonds, with the irradiation exposure, by the aid of a metal complex that is vulnerable to blue light and the presence of an electron receptor in the medium [30]. Keratose solutions were prepared in different buffers such as PBS (Phosphate Buffer Saline) and Tris-HCl. As an additive, glycerol was added onto specified solutions in order to stabilize the gel structure after crosslinking. As the cell culture tests made on NIH 3T3 mouse fibroblast cells have shown that, although the proliferation of the cells seeded on the hydrogels has been a little slower than the ones which have been seeded on blank tissue culture coated plates, at the end of hour 7, the majority of the hydrogels -especially the ones that have been prepared with PBS- have shown the same attachment percentages; which indicates that the prepared keratose hydrogels could be promising candidates to be used in tissue engineering applications. Finally, chemically crosslinked keratin materials can be discussed as a biomaterial preparation method. In a study that has been conducted by Tanabe et al., keratin derived materials were crosslinked with chemical agents, called as EDGE and GDE, in order to be cast as keratin film surfaces [59]. Several different keratin films were prepared with respect to different determined concentrations of cross linkers as well as with the addition of chitosan, to be able to compare the mechanical and cell adhesion/proliferation properties of different resulting biomaterials. The results have revealed that; all samples have shown similar mechanical strength. However, the chemically crosslinked films have had the ability to be stretched out a little bit further compared to the others. Also, since the cell cultures are known to grow well on slightly hydrophobic surfaces than the hydrophilic ones [60]; the hydrophilic medium that has been created in the presence of cross linkers may have negatively affected the fibroblast growth, as the attachment on the crosslinked films was seen to be lower than the keratin and/or chitosan films alone. Nevertheless, the cells which managed to attach did proliferate on the crosslinked films, proving that rather than cytotoxicity, the over-hydrophilicity could be responsible of the lower cell attachment levels.

Keratin based materials have a wide range of usage, from biomedical applications, to purification systems that possess fibrous components, to pharmaceuticals and even to adsorption systems. For tissue engineering, Silva et al., have compiled a table that includes the recent studies that is based on tissue engineering using keratin derived materials, on different cell cultures such as L929 mouse fibroblasts, Schwann cells,

vascular smooth muscles and hepatocytes [41]. Moreover, Reichl has conducted a detailed work, by using keratins as substrates for 12 different cell cultures, as well as testing different keratin coating methods [61]. Besides tissue engineering, keratins are mostly used in wound healing processes, and several studies that have focused on the topic can be found here [16,24,62]. Although the scope of the following study cannot directly be related with wound healing, Cruz et al., have conducted a work on peptide interaction of keratins, to understand the interaction characteristics of peptides that are present in hair-care products, in order to prevent or lessen the possible damages that can be done on human hair and/or scalp [63]. Drug and bioactive compound delivery can also be considered as a promising platform for the use of keratins, as several studies on this area of research are exhibited hereby [64,65]. At last but not least, apart from the discussed areas of research that have been mentioned up to know; Ki et al., have utilized silk reinforced keratin fibers to fabricate a membrane that is desired to be used in heavy metal adsorption, and stated that the applicability of these membranes were excellent as heavy metal adsorbents [66].

CHAPTER 3

MATERIALS AND METHODS

In this chapter, materials and experimental procedures used in this study were outlined. Firstly, materials needed for the syntheses along with their suppliers were described. Then, in the methods sub section, experimental protocols for keratose extraction, hydrogel preparation procedures and characterization techniques were given briefly, with their instrumental settings and details.

3.1. Materials

Wool samples from Akkaraman sheep breed (*Ovis aries* Linnaeus, 1758) localized in the Central Anatolian region of Turkey were kindly provided by Lalahan Livestock Central Research Institute (Ankara, Turkey) [67]. Chloroform, Tris-base and hydrochloric acid (HCl), ethanol (absolute grade), acetic acid, deuterium oxide, 2-(N-morpholino) ethanesulfonic acid (MES), sodium dodecyl sulfate (SDS), dimethyl sulfoxide (DMSO) and L-glutamine were purchased from Merck (Darmstadt, Germany). Methanol, Tris-HCl, sodium sulfide nonahydrate, sodium chloride, sodium phosphate monobasic, sodium hydroxide, FT-IR grade potassium bromide, peracetic acid solution (32 w% in dilute acetic acid), picrylsulfonic acid solution (5 w% in water), TruPAGE® precast gels (10x8 cm with 4-12% gradient), cellulose membrane dialysis tubing (43x27 mm, MWCO ~14000 Da), CCK-8 cell counting kit, tyrpsin-EDTA 0.25% solution, penicillin & streptomycin antibiotics solution, were obtained from Sigma-Aldrich (Sigma-Aldrich Co., St. Louis, MO, USA). fetal bovine serum (FBS), bovine serum albumin (BSA) and RPMI 1640 cell medium were gathered from Biological Industries (Cromwell, CT, USA). Cell Viability/Toxicity Live/Dead Assay kit were acquired from Biotium (Fremont, CA, USA). Sulfuric acid (96 %) and tetrakis (hydroxy methyl) phosphonium chloride (THPC) was provided by Panreac Quimica (Barcelona, Spain) and Acros Organics (Geel, Belgium), respectively.

Coomassie brilliant blue R-250 and PageRuler^{TM} Pre-Stained Protein Ladder products were purchased from and Thermo Fisher Scientific (Waltham, MA, USA). All solutions were prepared using deionized water if not stated otherwise.

3.2. Methods

3.2.1. Extraction of Keratose

Soluble fractions of wool proteins were extracted using peracetic acid oxidation, by following the reaction given in the Figure 2.6.a. Schematic diagram of keratose extraction procedure is given in Figure 3.1. Briefly, wool samples were intensively washed with deionized water in order to remove natural dirt and contaminants. 5 g of sample was placed in 500 ml of water at 50°C and was shaken at 150 rpm for a few hours. The procedure was repeated until a clean solution is obtained. Cleaned wools were defatted using Soxhlet extraction with a solvent mixture containing chloroform and methanol (79:21 % vol/vol) at its azeotropic temperature. For a 5 g sample, 250 ml of solvent was used and the extraction process was proceeded at least 6 h, maintaining a syphon rate of 6 hr^{-1}. Residual solvent in the defatted samples was removed by evaporating at room temperature in a fume hood followed by using a vacuum oven at 40 °C. Oxidation of the cysteines of the wool was performed by shaking 5 grams of dried fibers and 400 ml of peracetic acid solution (2% w/v) at 37 °C and 150 rpm overnight avoiding exposure to the light. The solution was filtered with a ceramic filter. To extract soluble proteins, the fibers were contacted with 200 ml 100 mM tris-base solution at pH 10.5 in an incubator at 37 °C with a shaking rate of 150 rpm for 3 h and the solution was filtered. This step was repeated two more times. Saved solutions were combined and pH of the resultant solution was adjusted to 4, using 1 N HCl solution. Precipitated proteins were isolated by centrifugation, washed three times with 100 ml 100 mM tris-HCl buffer at pH 4.2 and dissolved in 30 ml tris-base solution at pH 10.5. The protein solution was dialyzed against 4 L deionized water using a pre-treated dialysis membrane tubing with a MWCO of 14 kDa. Dialysis medium was changed thrice a day, and the dialysis process was carried out for 3 days. Finally, the dialyzed keratoses were frozen at -80 °C, lyophilized and stored at -20 °C.

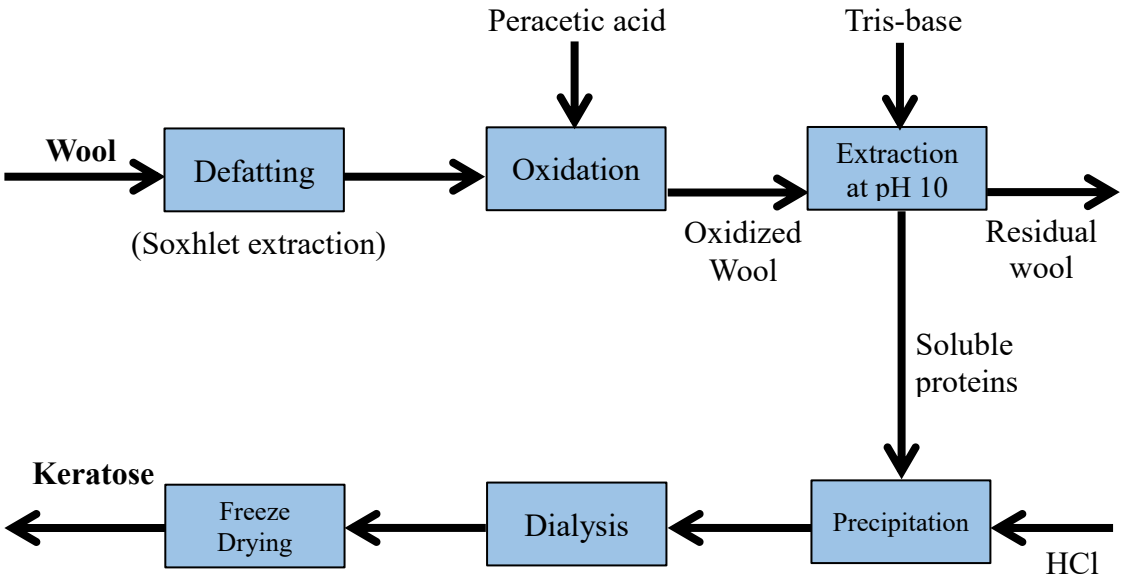

Figure 3.1. The flow diagram of keratose extraction process

3.2.2. Characterization of Wools and Extracted Keratose

X-ray Diffraction (XRD) analyses were carried out using a Philips PANalytical X'Pert Pro (Almelo, Netherlands) model diffractometer with an incident CuK_α radiation at 1.54 Å and scan rate of 0.139 °/min. The Bragg angle (2θ) values were changed between 5 and 80°.

Fourier Transform Infrared Spectroscopy (FT-IR) of the samples was performed on a Shimadzu 8400S (Tokyo, Japan) spectrophotometer using KBr pellet technique. The spectra were taken between 400 and 4000 cm^{-1} wavenumber range with a scan number of 32 and resolution of 2 cm^{-1}.

Scanning Electron Microscopy (SEM) images of the raw and processed wools were observed using a FEI Quanta 250 FEG (Oregon, USA) model instrument. The samples were prepared by cutting into fragments of several millimeters and vacuum drying at 40°C, followed by a sputter-coating of a gold layer in rarefied argon.

The surface of the samples was scanned at 3 kV. Mean diameter of the raw wool fibers was determined using ImageJ software [68] (NIH, US) by averaging the data from 30 different spots.

Thermal Gravimetric Analyses (TGA) of raw wool and keratose were conducted on a Shimadzu TGA-50 (Tokyo, Japan) model instrument between room temperature and 1000 °C at a 10 °C/min heating rate using N_2 atmosphere with a flowrate of 40 ml/min.

Sodium dodecyl sulfate polyacrylamide gel electrophoresis (SDS-PAGE) was carried out using a TruPage^{TM} precast gel with a gradient of 4-12%. Keratose solution at 10 mg/ml concentration in deionized water was incubated at 90°C for 5 min. A total volume of 10 µl sample was prepared by mixing 2 µl of protein solution with 8 µl sample buffer and the mixture was loaded and run through the gel using a buffer (with a composition of 1.2 M Tris-Base, 0.6 M MES and 2.0% w/v SDS) by applying a voltage of 180 V for 30 min. For visualizing the scale of the molecular weight on the gel, PageRuler^{TM} Pre-Stained Protein Ladder was used (Thermo Scientific, Waltham, MA, USA). The gel was, then, stained with Coomassie Brilliant Blue R-250 solution for 2 h and was destained with a solution containing 20% ethanol and 5% acetic acid for 3 h with successive washes.

3.2.3. Preparation and Characterization of Keratose Structures and Hydrogels

Amine content of keratose proteins was determined by TNBSA (2,4,6-trinitrobenzene sulfonic acid) assay. A TNBSA solution of 5% w/v was diluted 500-fold in 0.1 M sodium bicarbonate ($NaHCO_3$) solution and final pH was set to 8.5 via sodium hydroxide (NaOH). Then, 500 µL of keratose solutions with varying concentrations were prepared in Milli-Q water and 250 µL of diluted TNBSA solutions were added to each of them. The final solutions were incubated for 2 hours at 37 °C to provide the complete reaction of TNBS with the primary amines of the proteins. To stop reactions, 250 µL of 10% sodium dodecyl sulfate (SDS) in Milli-Q water and 1N HCl solutions were added to each sample. Finally, the absorbance was measured at 420 nm, and the corresponding amine group content was calculated as 1 x 10^{-2} mmol amine/g keratose using the extinction coefficient of L-glycine (22750 $M^{-1}.cm^{-1}$) [60].

Structures formed at low concentrations were investigated using dynamic light scattering (DLS) and atomic force microscopy (AFM) techniques. Keratose solutions were prepared at 5, and 10 mg/ml concentration using phosphate buffer saline (PBS; 10

mM phosphate containing 150 mM NaCl at pH 7.4) and filtered. The solutions were equilibrated at 25°C for at least 15 min prior to measurements. Diffusion coefficients of the samples were determined using CONTIN method and converted to corresponding hydrodynamic diameter values using Stokes-Einstein equation. DLS measurements were recorded using a Micromeritics NanoPlus model instrument with three measurements for each sample. 5 mg/ml keratose solution in DI water was used in AFM characterization. 3 µl of filtered solution was applied to freshly cleaved mica evenly and diluted with 10 µl of Milli-Q grade water. AFM imaging was performed at room temperature, using tapping mode with a Bruker silicon cantilever tip having a string constant around 0.1 N/m (Camarillo, CA, USA). AFM image of the sample was taken using a Digital Instruments-MMSPM Nanoscope lV model instrument and the images were analyzed using NanoScope Analysis software (Bruker, US).

Keratose hydrogels were prepared by dissolving keratose in an appropriate solvent (PBS at pH 7.4 or deionized water) at 10% w/v concentration (100 mg/ml) and 7.5% w/v concentration (75 mg/ml) for physical and chemical hydrogels, respectively. To get physical hydrogels, resultant solutions were incubated at 37 °C or 50 °C for 4 h to promote gelation. For crosslinked gels on the other hand, three sets of hydrogels were prepared, at amine group:crosslinker ratios of 1:1, 1:2 and 1:4. Proposed reactions of THPC crosslinking process are given in Figure 3.2. After gels were formed, the tube inversion tests were made to ensure that the resulting hydrogels were stable and solid-like.

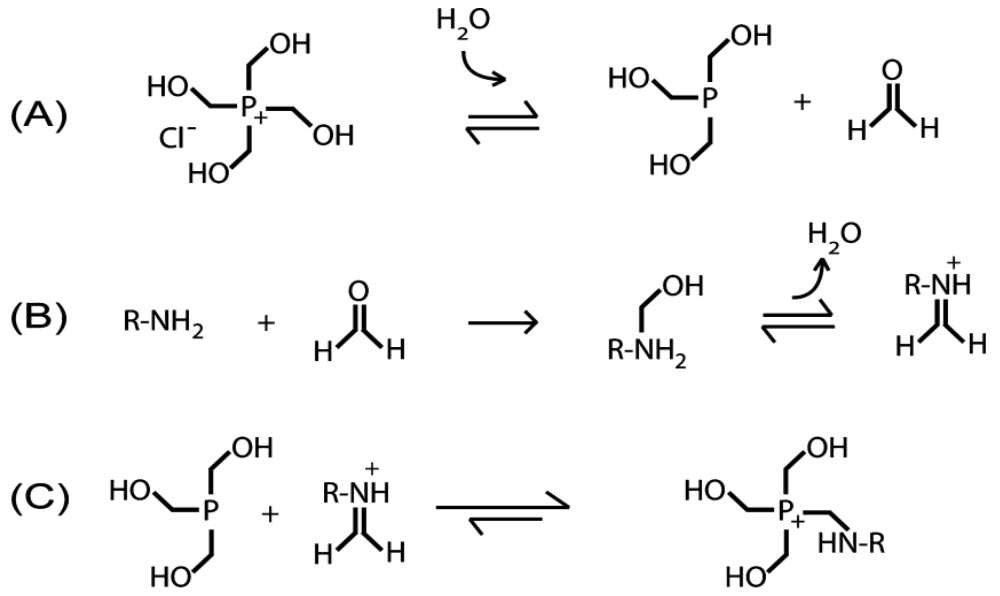

Figure 3.2. Proposed reactions of amine crosslinking by THPC; a) formaldehyde formation, amine fromaldehyde Mannich-type reaction, c) amine coupling completion (Source: [85])

Pore size and interconnectivity of the hydrogel networks were evaluated using FEI Quanta 250 FEG SEM (Oregon, USA) model instrument. Both sets of hydrogels that were prepared in deionized water were soaked into liquid N_2 and freeze-dried at -89°C in order to remove all the aqueous content. Images of top view and cross-sectionally fractured portion of the samples were observed in E-SEM mode. Average pore size of the hydrogels was determined, by measuring 30 pores from different spots using ImageJ software.

Secondary structures of the keratose powder, solutions and hydrogels were assessed using attenuated total reflection Fourier transformed infrared (ATR-FTIR) spectroscopy. Keratose solutions and hydrogels were prepared in D_2O, and hydrogels were freeze-dried before being analyzed. The experiments were conducted using a Perkin Elmer Spectrum Two instrument (Waltham, MA, USA). The data were acquired between 400-4000 cm^{-1} wavenumber range with a resolution rate of 4 cm^{-1} and scan number of 32. Amide I region was deconvoluted into optimum number of Gaussian peaks according to R^2 and χ^2 values using Origin data analysis and graphing software (OriginLab, Northampton, MA).

Oscillatory rheology experiments of the hydrogels were carried out on a Thermo Fisher Scientific HAAKE MARS Rheometer (Waltham, MA, USA) instrument equipped with a stainless steel parallel plate with a diameter of 250 mm. 700 µl of viscous keratose solution prepared in PBS buffer at pH 7.4 was applied to the plate. For physical hydrogels, the gap distance between the plates was adjusted to 200 µm and light mineral oil was used to block the sides of the plates to suppress the possible evaporation of the material during the hydrogelation and rheological tests. The temperature of the instrument was set as 37 °C or 50 °C and samples were allowed to undergo sol-gel transition inside the plates for 4 h. For physical hydrogels, the gap distance between the plates was adjusted to 200 µm and light mineral oil was used to block the sides of the plates to suppress the possible evaporation of the material during the hydrogelation and rheological tests. For the chemical hydrogels, after the keratose solutions were pipetted onto the plate, the temperature was decreased to 5 °C right before the cross linker was added in order to prevent a rapid sol-gel transition. Frequency sweep tests were performed between a frequency range of 0.1 and 100 Hz at a constant strain of 5% at 37 °C.

Cell proliferation and live/dead assays were performed using L929 mouse fibroblast cell line using three independent samples. The cells were cultivated in RPMI 1640 cell medium containing 200 mM glutamine, %10 fetal bovine serum (FBS), and penicillin and streptomycin antibiotics (50 unit/ml). The cells were sub-cultured every

other day and any of the fourth subcultures was used in the assays. Known weight of lyophilized keratose was sterilized by UV light for 1 h and 10 w/v % keratose solutions were prepared in sterile PBS buffer at pH 7.4. For cell proliferation tests, 100 µl keratose solution was pipetted into each well of a 96-well microplate and incubated at 37 °C to produce hydrogels. Collagen I and tissue culture treated empty wells were used for control. 30 µl of collagen I solution (40 µg/ml) prepared in sterile PBS was used to coat each well at 4 °C for 12 h. 100 µl L929 cell solution with a cell concentration of $1x10^5$ cell/well was added to each well and the microplates were incubated at 37 °C in 5% CO_2 atmosphere for 1, and 5 days. Cell medium of the wells were changed in every 2 days.

To determine cell proliferation, 10 µl of stock CCK-8 solution at 37 °C was added to each well and the microplates were incubated for 4 h. Absorbance values were measured at 450 nm using a Thermo Fisher Varioskan Flash microplate reader (Waltham, MA, USA). For live/dead assay, 100 µl of hydrogel prepared in the microplates using the same procedure as cell proliferation assay. Collagen I and blank tissue culture plastic wells were used as controls, and the cells were seeded on the hydrogels and control surfaces with an initial cell density of $1x10^5$ cells/well and incubated at 37 °C in 5% CO_2 atmosphere for 1, and 5 days. The cells were washed with serum free-medium and freshly prepared 1 µM calcein AM in anhydrous dimethyl sulfoxide (DMSO) and 2 µM ethidium homodimer III in DMSO/H_2O, prepared in sterile PBS solution were added into the wells. The microplates were incubated for 45 minutes. Excitation wavelengths were used as 493 nm and 592 nm for calcein AM and ethidium homodimer III, respectively. Labeled cells were monitored and cell images were taken using a Zeiss Axiovert 200M model fluorescence microscope (Oberkochen, Germany). Statistical analyses were carried out using independent two-sample t-test method on Minitab software. p-value<0.05 obtained from pairwise comparison of the samples was considered as statistically significant difference.

CHAPTER 4

RESULTS AND DISCUSSION

In this chapter, the experimental results are given. Firstly, the characterizations of wool and keratose proteins were reported. Characterization results of nanostructures formed at low keratose concentrations were presented. Rheological, morphological and conformational behavior of physical and chemical hydrogels were determined. Finally, as a preliminary study, cell adhesion and cytotoxicity properties of a select hydrogel are evaluated, by the aid of OD measurements and fluorescence microscopy images taken to visualize the cell viability and proliferation of the given cell line, L929 mouse fibroblasts.

4.1. Characterization of Wool samples and Extracted Keratose

4.1.1. Fourier Transform Infrared Spectroscopy (FT-IR)

Functional groups and structural changes that occurred during the extraction of keratoses were determined using FTIR spectroscopy and the spectra of defatted raw wool, oxidized wool and keratose are presented in Figure 4.1. Fingerprints of proteinaceous structure were revealed by amide I (1600-1690 cm^{-1}), amide II (1480-1575 cm^{-1}), and amide A (~3300 cm^{-1}) bands were observed for all wool samples and keratose [69]. Additionally, a new band observed for oxidized wool and keratose at around 1040 cm^{-1} corresponds to asymmetric vibrations of S-O groups of the sulfonate in cysteic acid confirmed the peracetic acid assisted oxidation of cysteines to cysteic acids [70,71]. However, in these spectra symmetric vibrations of S-O groups of the cysteic acid about 1075 cm^{-1} manifested as a weak band [70]. The sharp band observed around 1657 cm^{-1} in the spectrum of keratose indicated the extracted protein is rich in α-helical secondary structure as the other α-keratin family of proteins [17,72,73].

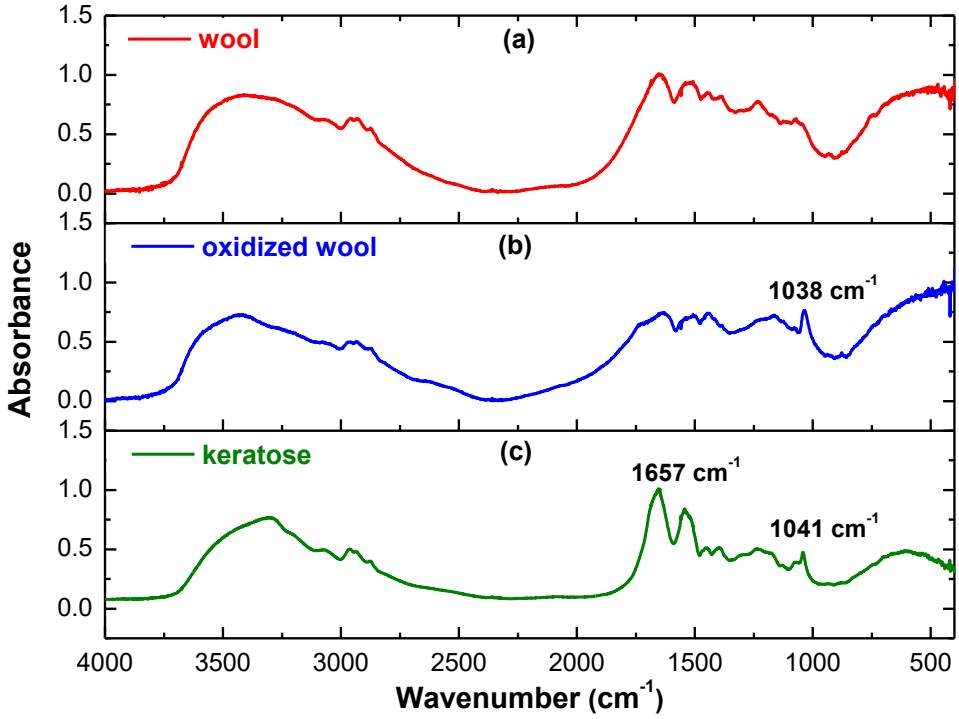

Figure 4.1. FT-IR spectra of a) defatted *Ovis aries* wool, b) oxidized wool and c) keratose protein, drawn in wavenumbers between 400-4000 cm^{-1}.

4.1.2. X-ray Diffraction (XRD)

XRD technique was used to detect crystallinity of the samples and fate of the ordered structures of the proteins during extraction process. XRD diffractograms of defatted wool, oxidized wool and extracted keratose are given in Figure 4.2. The patterns indicated that all the samples are semi-crystalline with a background representing amorphous fractions associated with broad peaks and matched to the patterns observed for α-keratins, as expected [74]. The peaks are more apparent for oxidized and extracted samples suggesting higher content of ordered structures. Similarly, intensities of the XRD peaks are higher for the keratin extracted using L-cysteine at basic pH compared to the parent wool sample [75]. However, the study of Zhang and colleagues implied that acid hydrolysis of wool using 4 N HCl at high temperature yielded amorphous structure [19]. The peak at 20° corresponds to β-sheet structure whereas the other peak at 9° represents both α-helical and β-sheet conformations of the proteins [75,76].

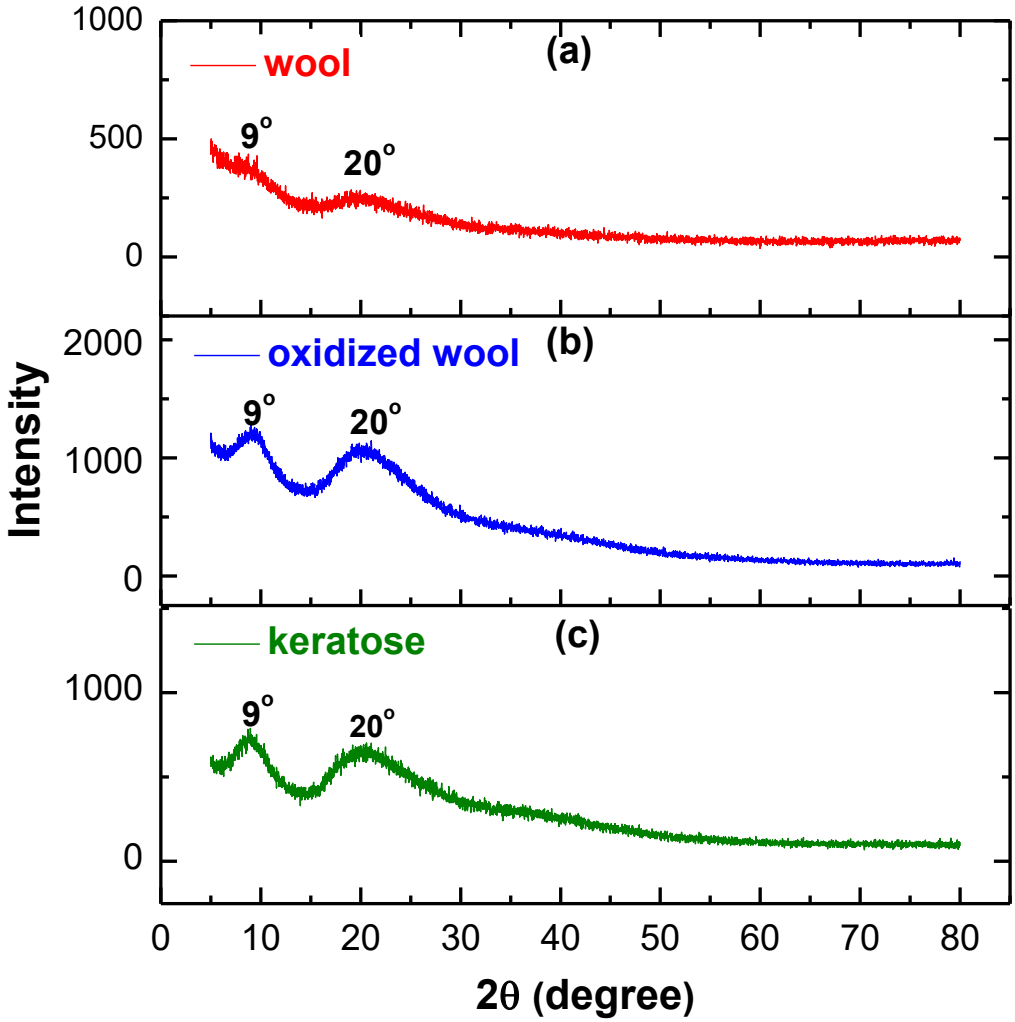

Figure 4.2. X-Ray diffractograms of a) defatted *Ovis aries* wool, b) oxidized wool and c) keratose proteins

No significant changes were observed between relative intensities of these two peaks for the oxidized wool and keratose indicating no detectable conformational changes during the extraction of keratoses from the oxidized wool. Thus, it is likely that the oxidation procedure applied in this study, did not give irreversible damages to the ordered structures of keratinous proteins.

4.1.3. Thermal Analyses

Thermal behavior of defatted wool and keratose were investigated using TGA method and the resultant TG and DTG curves are given in Figure 4.3. All three samples exhibited three major thermal transitions by giving less than 2% residue at the end of

1000 °C. The first endotherm observed around ~75 ± 3 °C corresponds to removal of moisture and volatile materials which constitutes ~6.5-7 % of the total mass of the samples. The second endotherm were obtained between 200 and 400 °C mainly indicating the degradation of side chains of the proteins [73,75,76]. In this region, the corresponding mass losses are; 36, 37, and 45 % for defatted wool, oxidized wool and keratose, respectively. Similarly, ~45 % mass loss associated with the second endotherm was reported for keratin from bovine hoof [75]. For keratose there exists a shoulder about 246 °C quite apparent within this endotherm which is probably due to the elimination of sulfur containing gases or other small molecules in a more cooperative manner compared to the wools. The last endotherm was observed between 450 and 600 °C and can be attributed to pyrolytic decomposition as suggested based on sudden contraction in DMA curve due to cyclization reactions [76].

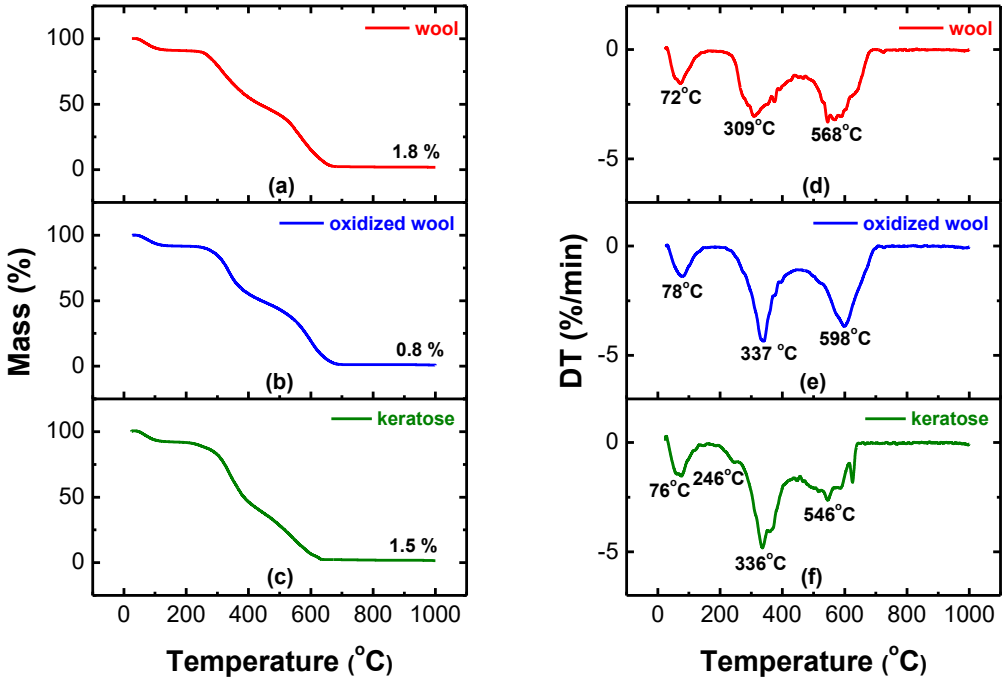

Figure 4.3.TG curves of a) defatted wool, b) oxidized wool, c) keratose, and corresponding DTG curves of d) defatted wool, e) oxidized wool, and f) keratose.

4.1.4. Scanning Electron Microscopy (SEM)

SEM pictures of defatted and oxidized wool and residual material after the extraction of keratose are given in Figure 4.4. Defatted wool fibers were observed to be stiff and polydisperse with an average diameter of 29 ± 10 μm. After the peracetic acid treatment, the oxidized fibers became more flexible and porous, indicating that di-sulfide bonds were broken. Extraction from keratoses, on the other hand, disrupted the fiber structures as clearly indicated by Figure 4.4.c. In consistent with this study, SEM images of the residual β-keratin rich structures of wools indicated that keratose proteins were not gently stripped from the wool fibers [71]. Conversely, hair fibers subjected to oxidation and extraction processes were split longitudinally [52].

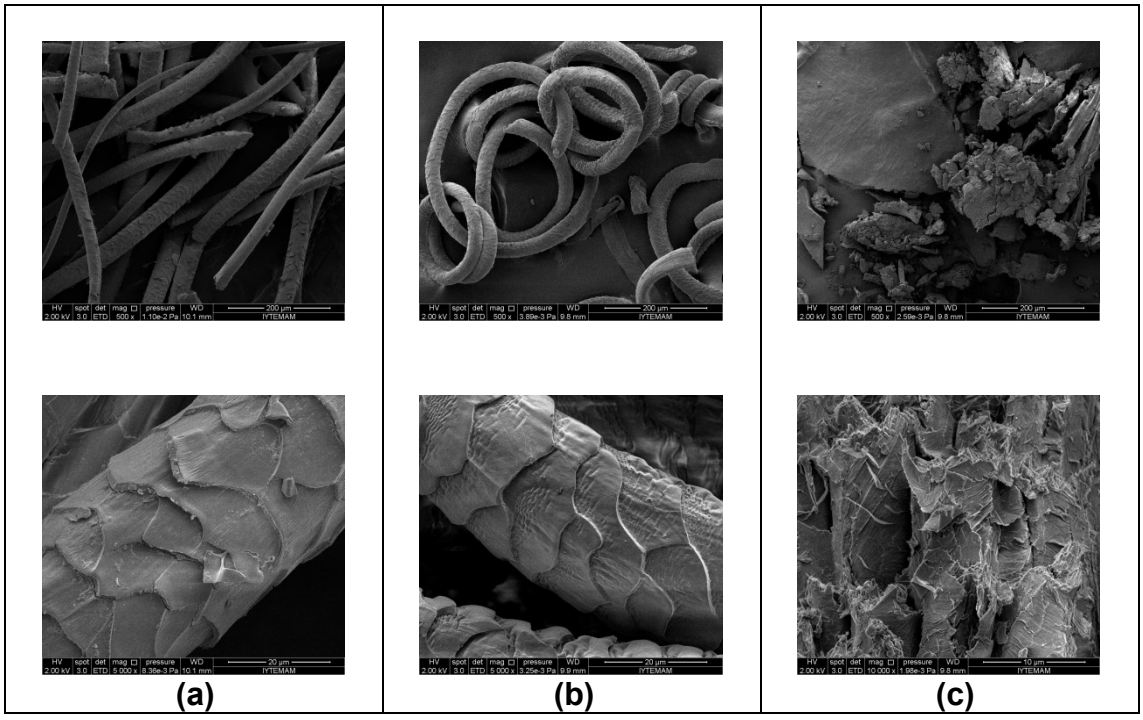

Figure 4.4. Scanning electron microscopy images taken for a) raw wool, b) oxidized wool and c) wool residue after extraction.

4.1.5. Molecular Weight Determination of Keratose

SDS-PAGE analysis results of the extracted keratin based proteins are given in Figure 4.5 and indicated a number of protein fractions populated between 14 and 100 kDa in diffusive manner rather than discrete bands. Relatively intense band between ~43 and

~53 kDa matched to the molecular weight distribution of monomeric α-keratose fractions extracted from a merino wool identified using LC-MS/MS [30]. The more distinct band was observed between ~23 and 33 kDa. It was reported that wool fibers also contain γ-keratin with high sulfur content and high tyrosine proteins in addition to α-keratins (low sulfur proteins). For merino wool molecular weight of γ-keratin were determined as 10.4 kDa and no traces of tyrosine rich proteins were observed upon following similar oxidation process applied in current study [30]. Therefore, the bands between ~23 and 33 kDa is likely due to the fragments of α-keratose formed during oxidation as peracetic acid can cleave peptide bonds.

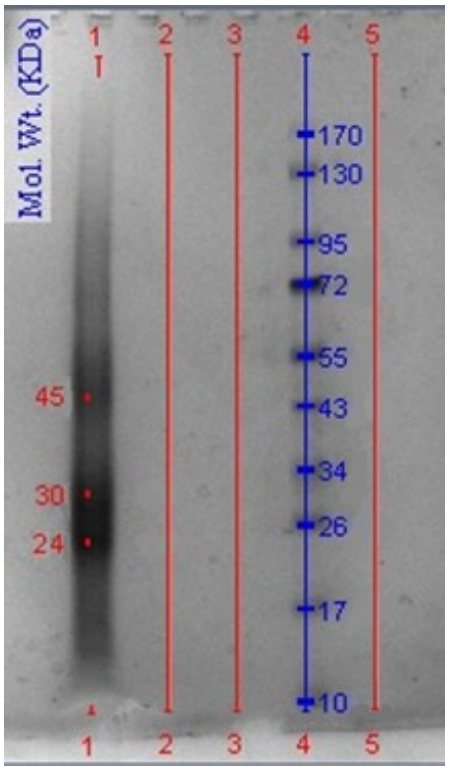

Figure 4.5. SDS-PAGE pattern of keratose proteins [Molecular weights given in kDa]

4.2. Characterization of Nanostructures Formed at Low Keratose Concentrations

Dynamic light scattering and atomic force microscopy were used to determine size and morphological characteristics of the structures formed at 5 and 10 mg/ml keratose solutions. Size distributions measured by DLS are given in Figure 4.6. Mean

hydrodynamic diameter values of the samples at 5 and 10 mg/ml concentrations were obtained as 25 ± 2 and 28 ± 1 nm, respectively. 2D AFM image and particle size distribution of 5 mg/ml sample are presented in Figure 4.7. Particles having ellipsoidal cross section with sizes between 25 and 40 nm were observed in consistent with DLS measurements.

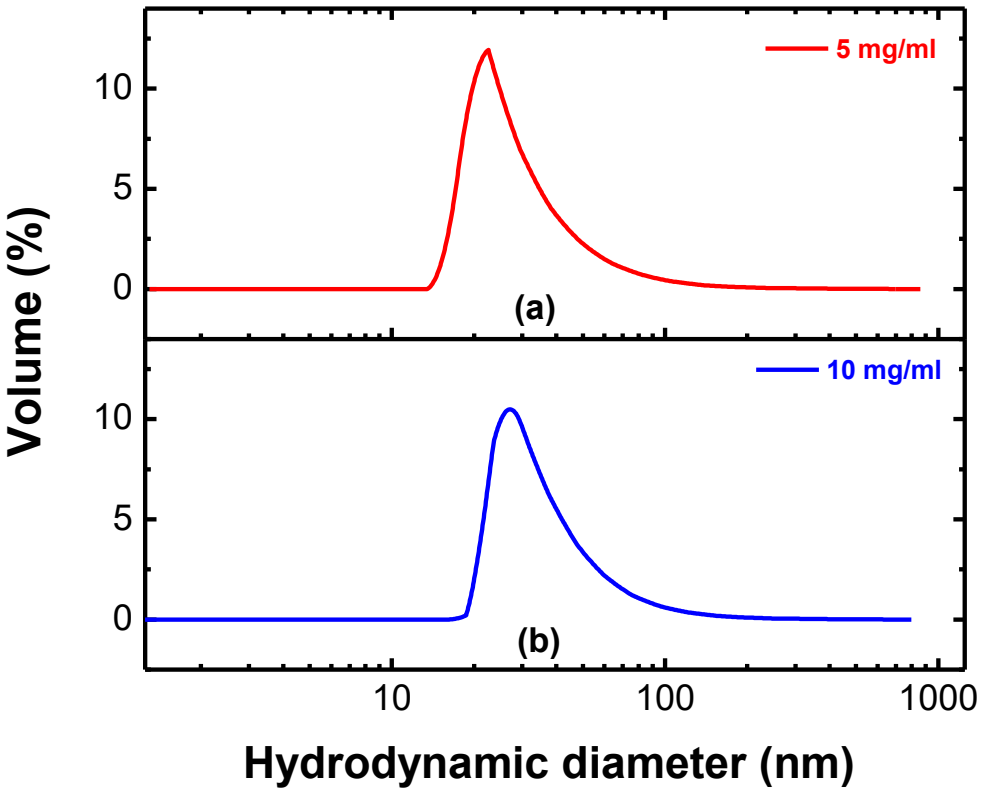

Figure 4.6. Size distribution of keratose solutions with concentrations a) 5 mg/ml, and b) 10 mg/ml.

G-actin monomer with similar molecular weight (~ 42 kDa) as α-keratin exhibited a hydrodynamic diameter of 5.8 nm, quite lower than those obtained in current study [77]. Hydrodynamic diameter of a fibrous protein, fibrinogen (MW = 340 kDa) was determined to be 22 nm [78]. Comparing size and molecular weight distributions of keratose with those of G-actin and fibrinogen and considering the DLS and AFM results, it can be suggested that keratoses at low concentrations in the solution form self-assembled into globular aggregates. Similar aggregation tendency was also reported for keratin (reduced form) samples that extracted from West Yorkshire region (UK) white sheep wool. Mean sizes (hydrodynamic diameter) of the keratin solution at 1 mg/ml concentration were found to be increasing from 14 to 30 nm as salt concentration increases from 5 mM to 0.5

M. Cryo-TEM image indicated ellipsoidal structures with a diameter of 12 and 44 nm at 5 mM salt concentration [79]. Mean sizes (hydrodynamic diameter) of the keratin solution at 1 mg/ml concentration were found to be increasing from 14 to 30 nm as salt concentration increases from 5 mM to 0.5 M. Cryo-TEM image indicated ellipsoidal structures with a diameter of 12 and 44 nm at 5 mM salt concentration [79].

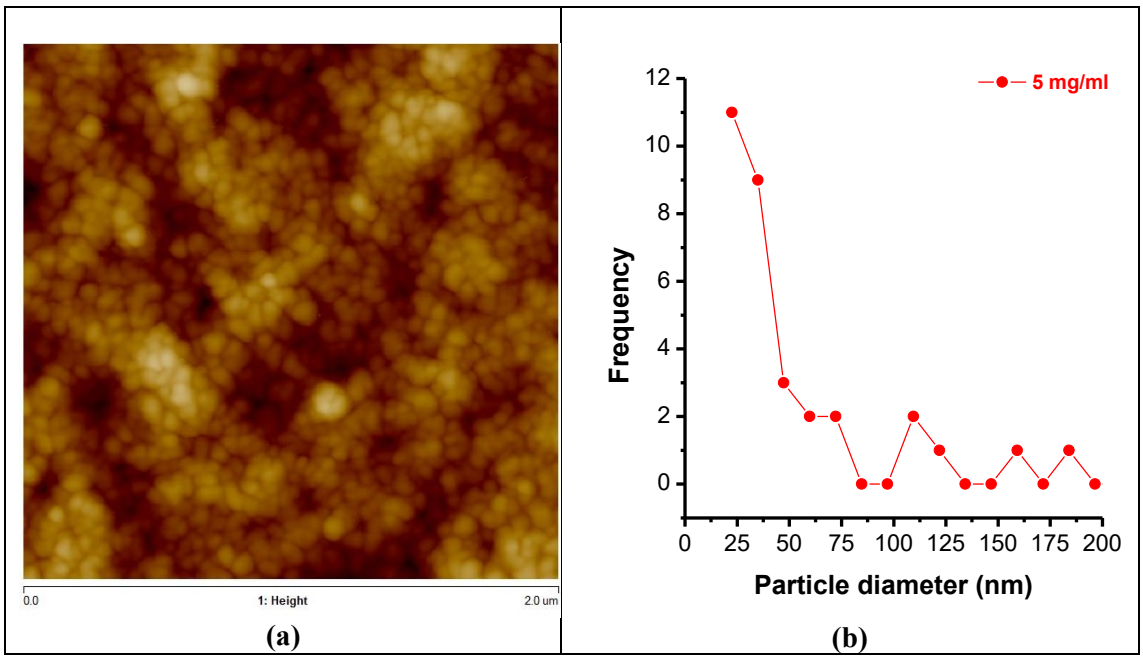

Figure 4.7. a) 2D AFM image, and b) particle size distribution of keratose prepared at 5 mg/ml.

4.3. Characterization of Physical and Chemical Hydrogels Formed at High Keratose Concentrations

4.3.1. Rheological Studies

Keratose solutions prepared at 100 mg/ml (10 w/v %) concentrations formed self-standing hydrogels upon incubation at 37 or 50 °C, whereas solutions prepared at 75 mg/ml (7.5 w/v %) were gelated by the addition of a chemical crosslinking agent, THPC. Rheological properties of the hydrogels were evaluated using oscillatory frequency sweep experiments. Linear viscoelastic response of hydrogels were evaluated and plots of frequency dependence of moduli are given in Figures 4.8 and 4.9. For each hydrogel sample, a frequency range of 0.1 to 100 Hz was selected and the corresponding G' (elastic

moduli) and G'' (loss moduli) of the samples were plotted and linear equilibrium modulus plateau were determined. As revealed from plots that, G' (storage modulus) values were obtained to be higher than G'' values (loss modulus) for each hydrogel sample tested, confirming their gel-like behavior. Thus, for all samples, the δ values (where; $\frac{G''}{G'} = \tan(\delta)$) of both gels are found to be closer to 0° than 90°, ensuring that the materials can be described as solid-like elastic gels. For the physical hydrogels, plateau G' values were obtained as ~100 Pa and ~1000 Pa for the respective hydrogels prepared at 37 °C and 50 °C. Stronger chitosan based gels were also obtained upon increasing temperature and enhanced mechanical strength was attributed to the increase in hydrophobic attractions. Increasing temperature, on the other hand, decreases strength of hydrogen bonds. Although breaking hydrogen bonding seems unfavorable, it may provide chain flexibility to create contacts by facilitating the formation of network structure as suggested for chitosan hydrogels [82]. In another study, human hair derived keratin and keratose based hydrogels were prepared at 20 w/v % concentration and 37 °C. Not surprisingly, higher G' value (~120 Pa) was obtained for the hair-based keratose hydrogel indicating that changing polymer concentration can be another parameter to tune the mechanical strength of the resultant hydrogels [52].

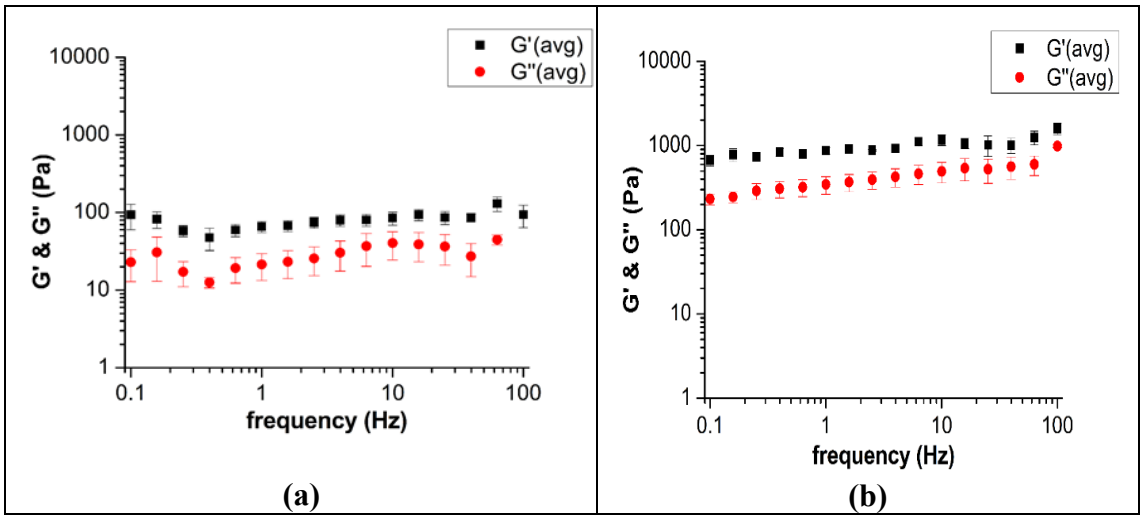

Figure 4.8. Frequency sweep data of self-assembled keratose hydrogels prepared at; a) 37 °C, b) 50 °C.

Also, in a similar area of interest, Ham et al. [55] have prepared different hydrogels containing various portions of both keratin-based proteins kerateine and keratose. They obtained 15% w/v self-assembled keratose hydrogels at 37 °C having a

G' value around 1000 Pa. For further comparison, storage moduli (G') of self-assembled keratin based hydrogels, prepared at various conditions are given in Table 4.2. Plots of frequency dependence of complex viscosity values of the hydrogels are represented in Figure A.1 in the Appendix A section. Decrease in complex viscosity with increasing frequency indicates shear thinning property of these hydrogels as observed in many other self-assembled hydrogel systems [83].

Table 4.1. Comparison of storage moduli of physical hydrogels.

Hydrogel material	Weight %	Assembly Temp. (°C)	Storage Modulus (kPa)	Reference
Kerateine	10	37	~0.3	[84]
Keratose	20	37	~0.15	[52]
Keratose	10	37	~0.1	This study
		50	~1	
Keratose	15	37	~0.8	[55]

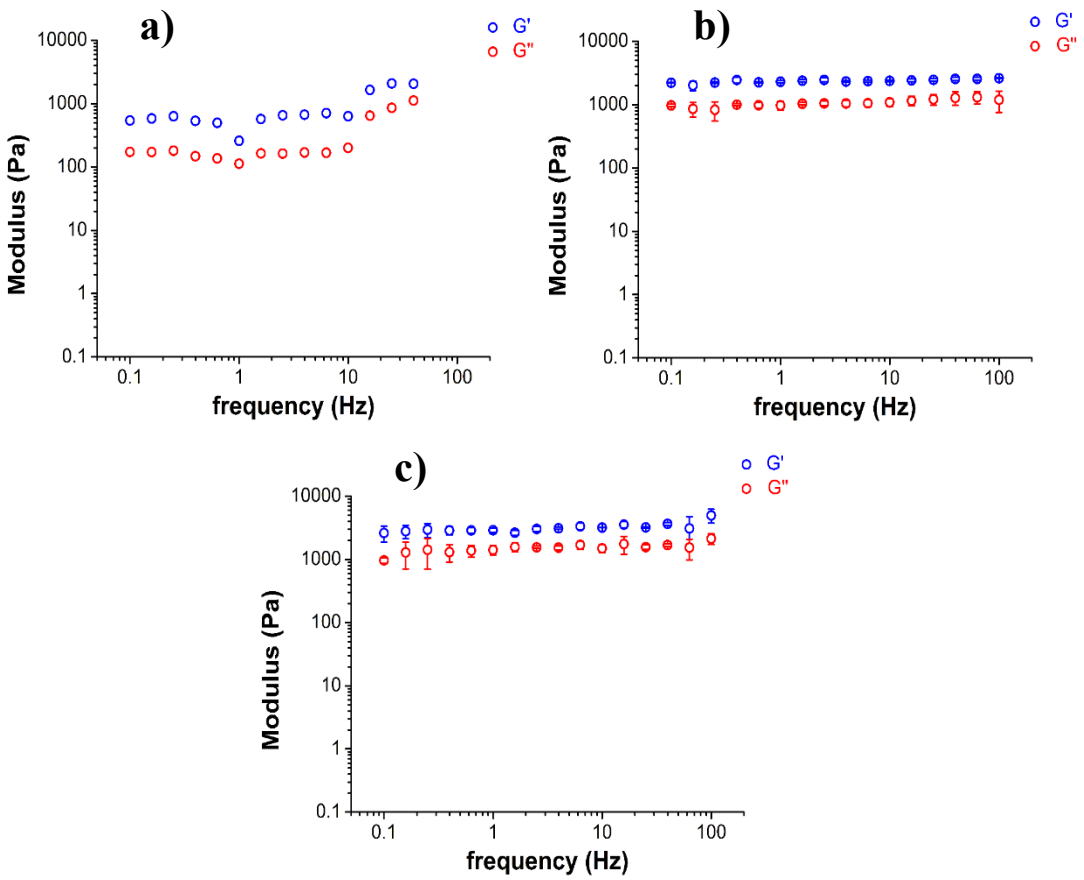

Figure 4.9. Frequency sweep measurements of chemically crosslinked keratose hydrogels, with the aminegroup:crosslinker ratios; a) 1:1, b) 1:2, and c) 1:4.

Oscillatory frequency sweeps were also performed on the chemical crosslinked gels, and the plots are given in Figure 4.10. A G' range between 1 and 5 kPa were achieved, by changing the amine group:crosslinker ratio from 1:1 to 1:4 An obvious increase in the G' values were oabtained, with the increasing crosslinker amount, as expected. Similarly, Chung and co-workers have used THPC to produce protein based hydrogels to be used as scaffolds and at the same protein concentration, increasing the crosslinker amount led to an increase in the storage moduli of the resulting hydrogels [85]. For a further comparison, chemical crosslinked protein hydrogels reported in the literature, with their corresponding crosslinker types and resulting G' values are tabulated in Table 4.3. When the amine group:crosslinker ratio is 1:2 or above, the storage moduli of the hydrogels prepared in the current study could be considered as moderately high compared to other proteins, except silk which was reported to be mechanically superior numerous times in the previous studies [33,86].

Table 4.2. Comparison of storage moduli of chemical hydrogels.

Hydrogel material	**Weigth %**	**Crosslinker**	**Storage Modulus (kPa)**	**Reference**
Recombinant Silk	5	APS+Rubpy	~8	[86]
Gelatin	5	EDC	~1	[87]
Keratose	7.5	THPC (1:1)	~1	This study
		THPC (1:2)	~2.6	
		THPC (1:4)	~5	
ELP	5	THPC (0.5:1)	~0.25	[85]
		THPC (1:1)	~1.2	

4.3.2. Microstructure of Hydrogels

SEM pictures of physically crosslinked gels prepared at 37 and 50 °C are given in Figure 4.8 and 4.9, respectively. Additional images of the same hydrogels are given in Appendix A section, in Figure A.2. For both physically constructed hydrogels, a distribution of pores ranging from ~2 μm to ~ 20 μm was obtained. From the top view of the hydrogels, mean pore sizes were measured as 6 ± 4 μm and 7 ± 4 μm for the hydrogels prepared at 37 °C and 50 °C, respectively. Cross sections of the freeze dried hydrogels indicated that network was constituted by fibrils. Thicker fibrils were observed in the structure of the hydrogel prepared at 50 °C. Hair-derived keratose at 20 w/v %

concentration was reported to have an average pore size of 13 ± 1 µm as given in an aforementioned study [52]. Higher pore size obtained at high keratose concentrations can be due to stronger interactions between the keratose molecules. Pore size and architecture have direct effect on cell proliferation and migration and optimum pore size depends on the cell type. Considering its optimum pore size given as 5-15 µm for tissue regeneration, keratose based hydrogels seem suitable for fibroblast ingrowth [80].

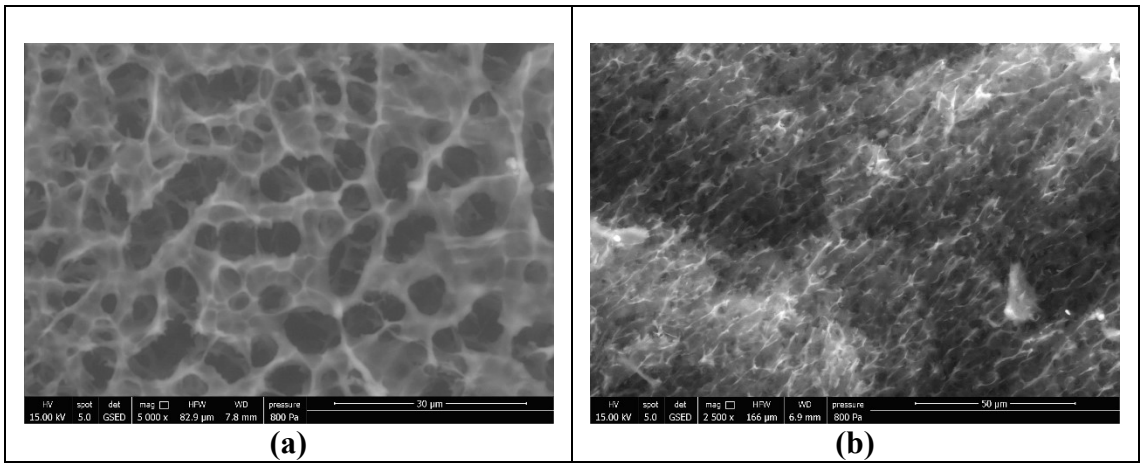

Figure 4.10. SEM pictures of freeze-dried physical keratose hydrogel prepared at 37 °C; a) top view; scale bar = 30 µm and b) cross section; scale bar = 50 µm.

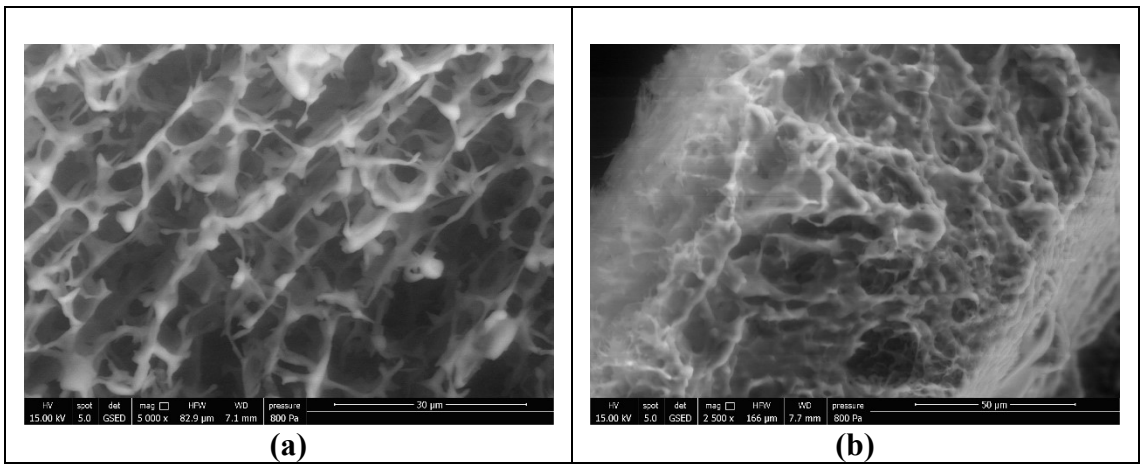

Figure 4.11. SEM pictures of freeze-dried physical keratose hydrogel prepared at 50 °C a) top view; scale bar = 30 µm and b) cross section; scale bar = 50 µm

Microstructures of chemically crosslinked hydrogels obtained using SEM are represented in Figures 4.11, 4.12 and 4.13, for corresponding amine group:crosslinker ratios of 1:1, 1:2 and 1:3, respectively. Supplementary images of these hydrogels are also represented in Appendix A section, in Figure A.3. Images of the hydrogels that have 1:1

amine:crosslinker ratio indicated that the gel network is consisted of thin-walled keratose fibers, with well-defined crosslinking points (Figure 4.10). Cross-sectional SEM image confirmed the presence of a 3-dimensional, interconnected network. As the amine:crosslinker ratio increased from 1:1 to 1:2 and to 1:4, the thickness of the pore walls was significantly increased, showing a flaky morphology rather than fibrous characteristics. Pore sizes tended to decrease, with values of 24, 14 and 11 μm for corresponding amine:crosslinker ratios of 1:1, 1:2 and 1:4, respectively. In consistent with our study, Jang and colleagues have previously reported a decrease in the pore sizes of PEG hydrogels, as the amount of crosslinking agent increased [81].

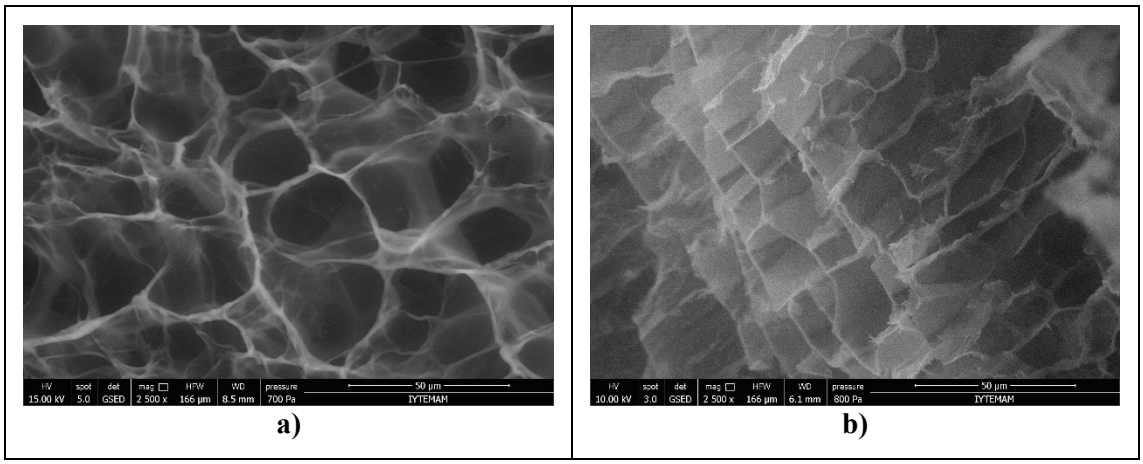

a) **b)**

Figure 4.12. SEM pictures of freeze-dried chemical keratose hydrogel prepared with 1:1 amine group:crosslinker ratio a) top view; scale bar = 50 μm and b) cross section; scale bar = 50 μm.

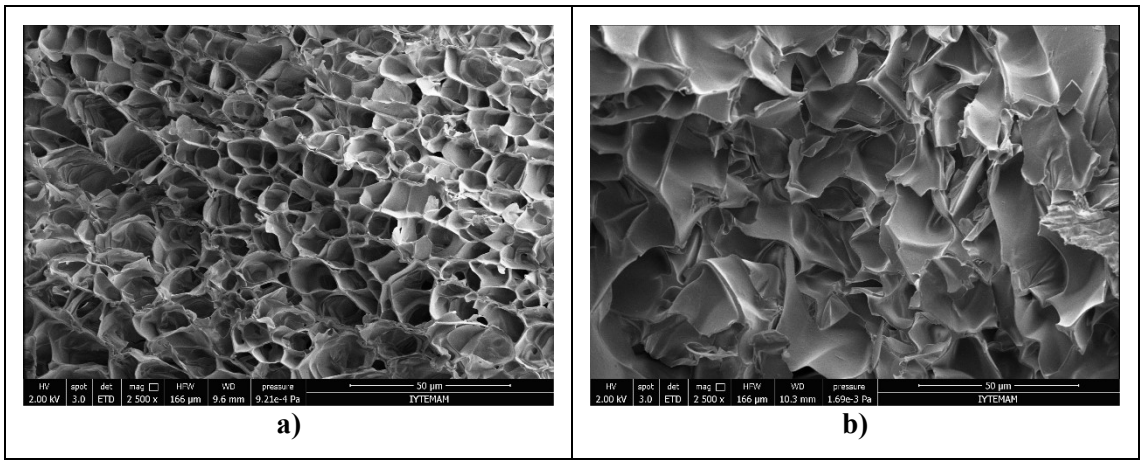

a) **b)**

Figure 4.13. SEM pictures of freeze-dried chemical keratose hydrogel prepared with 1:2 amine group:crosslinker ratio a) top view; scale bar = 50 μm and b) cross section; scale bar = 50 μm.

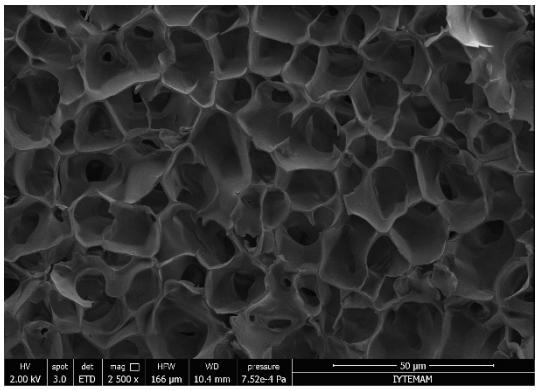

a)

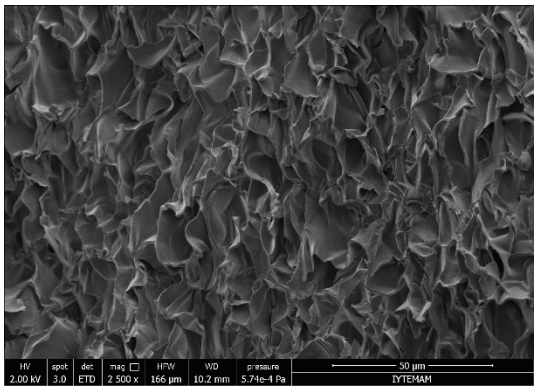

b)

Figure 4.14. SEM pictures of freeze-dried chemical keratose hydrogel prepared with 1:4 amine group:crosslinker ratio a) top view; scale bar = 50 µm and b) cross section; scale bar = 50 µm.

4.3.3. Cell Studies

4.3.3.1. Cell Proliferation Study

As a preliminary study, cell interactions of keratose hydrogels were tested by monitoring the behavior of L929 mouse fibroblast cells seeded on self-assembled keratose hydrogels which were pre-formed at 37 °C. In order to conduct the proliferation test, CCK-8 assay was used. As control samples, the cells were also seeded on collagen I coated and bare tissue cultured plastic wells, with the same cell density. Comparison of absorbance values of the keratose hydrogel and control samples for the 1st and the 5th day of cultivation are given in Figure 4.15. p values obtained from pair-wise comparison of the samples are tabulated in Appendix A section in Table A1. After 1 day of seeding, absorbance values measured for collagen and keratose hydrogels were found to be higher than the untreated well ($p < 0.05$). Statistical comparison of keratose hydrogel and collagen indicated that no significant difference in their abilities to promote cell proliferation ($p > 0.05$). However, at the end of day 5; absorbance for all the cell supporting media were comparable with similar standard deviations ($p > 0.05$), suggesting that keratose hydrogels could support cell attachment and proliferation as much as collagen and tissue culture plastic material. Growth rate of L929 mouse fibroblast cells seeded on keratin sponges were reported to be higher than that of a

commercially available plastic culture dish and this observation was attributed to the presence of cell-binding sequences that are present in the amino-acid sequence of the keratin extracted from wool [29].

4.3.3.2. Cell Viability and Toxicity

Morphology and distribution of the seeded cells were monitored by the aid of fluorescence microscopy after dyeing them with both calcein AM and ethidium homodimer III fluorescent dyes. Corresponding fluorescence microscopy images are given in Figure 4.16 and 4.17. At the end of day 1, homogenous distributions of L929 cells were obtained on both collagen and tissue cultured plastic cell supporting media. Cells were observed to be mostly round in shape, and low number of cells were morphed into the known spindle shape [84]. Additionally, the 3D rendering images have revealed that, the live/dead cell ratio for the fibroblasts is relatively higher for collagen medium, when compared with the tissue cultured plastic. Unfortunately, it was not possible to get decent images of keratose hydrogel, which can be attributed to high thickness of the prepared hydrogel. It is also possible that seeded cells could have diffused inside of the 3D hydrogel complex. Although the staining was not successful for the keratose hydrogel, the optical images indicated that there exist L929 cells inside the protein hydrogel matrix.

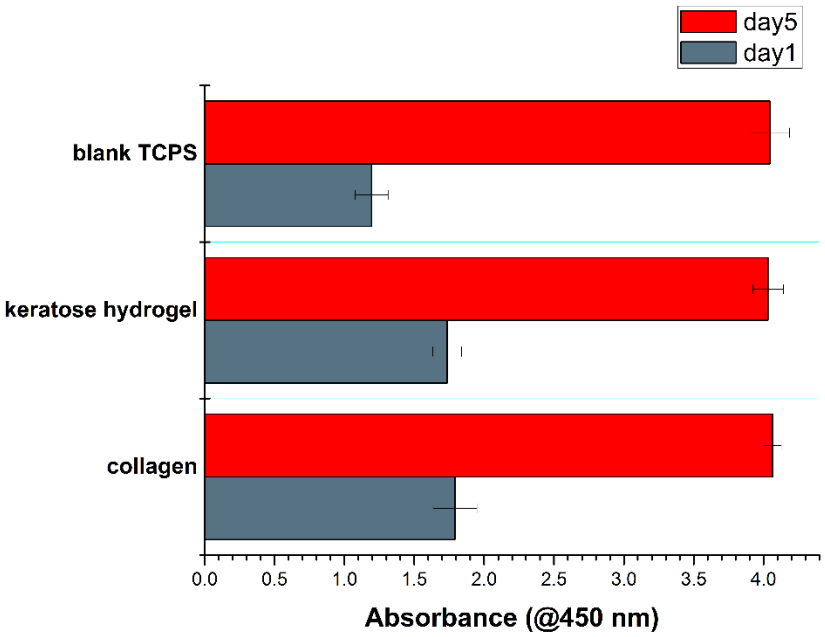

Figure 4.15. Absorbance read at 450 nm for CCK-8 assay of L929 cells, seeded on various samples at 1 and 5 days after cultivation

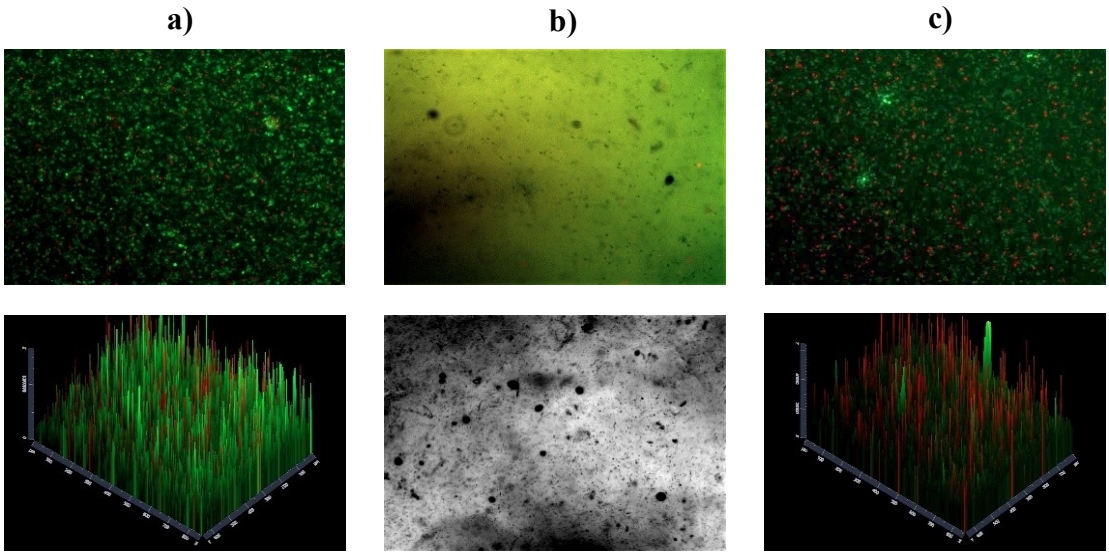

Figure 4.16. Fluorescence microscopy images of L929 cells seeded on; a) collagen, b) 10% w/v 37 °C keratose hydrogel and c) blank TCPS at cultivation day 1

Compared to day 1, images taken at day 5 revealed that cells seeded on tissue cultured plastic and collagen proliferated significantly. Cells seeded on hydrogels were also more visible when compared to day 1, due to the fact that the dyeing time were increased from 35 minutes to an hour.

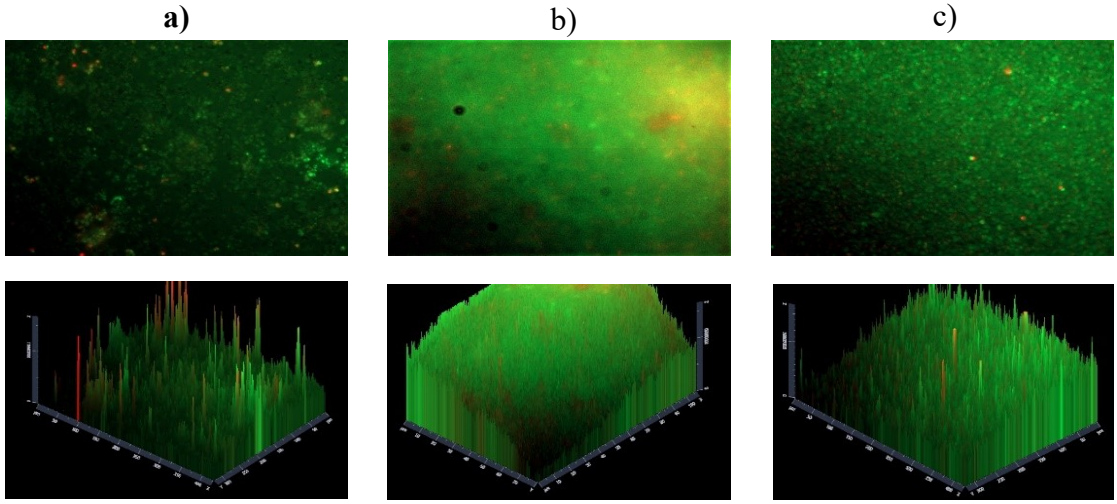

Figure 4.17. Fluorescence microscopy images of L929 cells seeded on; a) collagen, b) 10% w/v 37 °C keratose hydrogel and c) blank TCPS at cultivation day 5

Similar to what was achieved in the current study, Wang and co-workers have conducted a similar work by using collagen, keratin and TCPS blank media for cell seeding, and reported that the highest amount of cell attachment was seen in tissue cultured flasks, while cells seeded on keratin based hydrogels formed clusters with a non-uniform distribution around the hydrogel surface [84].

4.4. Conformational Analysis of Keratoses in Different Forms

Molecular conformations at different conditions have been frequently evaluated by using FT-IR spectroscopy. Although H2O is a preferable solvent because of its inertness, due to its the strong IR absorbance in Amide I region [69], the overlap with the secondary conformation peaks of the proteins can be unavoidable. Thus, keratose samples were dissolved in D2O or freeze dried, in order to eliminate any spectral interference that comes from O-H bending vibrational band. To evaluate the secondary structure of the samples, deconvolution of Amide I region (1600-1700 cm-1) of FT-IR spectra of the protein samples was carried out. In this specified region where the origin of the peaks are directly related with the C=O stretching vibrations of the corresponding proteins, the idiosyncratic peaks describing different secondary structures can be resolved.

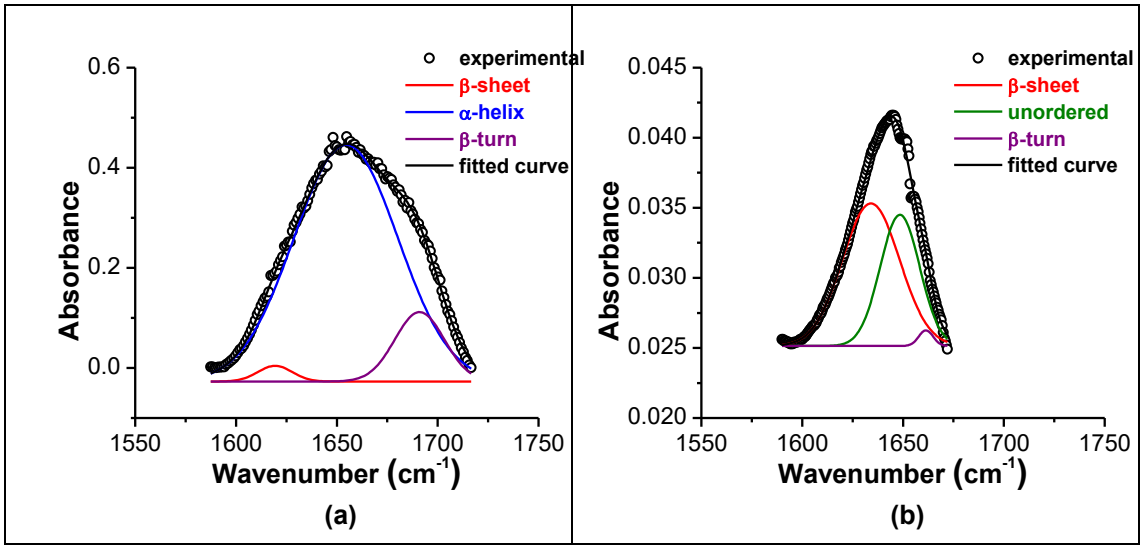

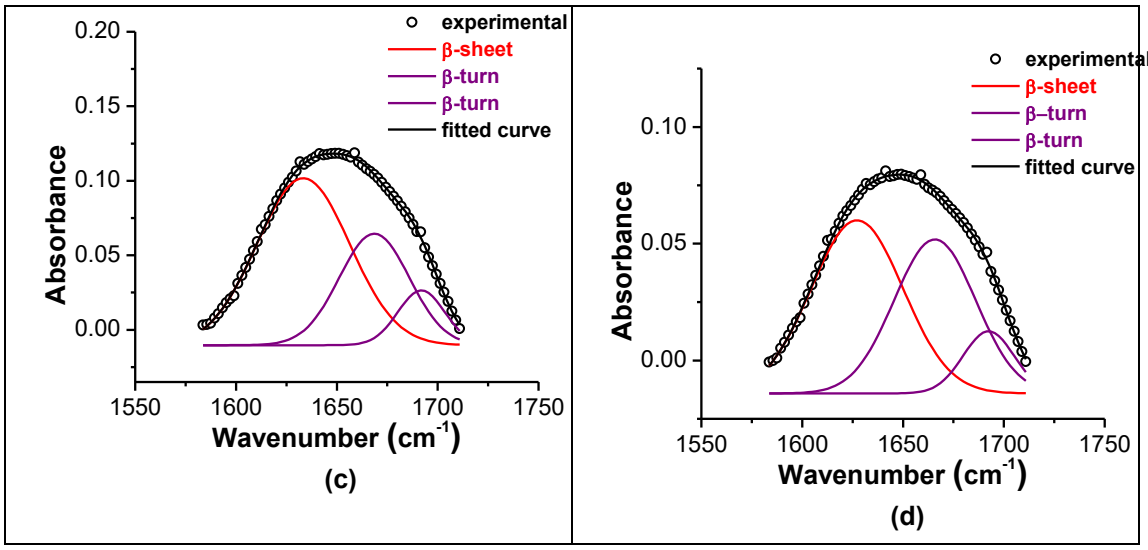

Figure 4.18. Deconvoluted amide I bands of a) keratose in solid form, b) 2 w/v % keratose solution in D_2O, c) freeze dried 10 w/v % keratose hydrogel prepared at 37 °C, and d) freeze dried 10 w/v % keratose hydrogel prepared at 50 °C.

Raw spectra of the keratose proteins in solid and solution form (2 w/v %), and freeze dried hydrogels prepared by physical and chemical crosslinking were deconvoluted into Gaussian peaks and resulted fittings were analyzed for the compositions of the corresponding secondary structures. Figure 4.18 shows the deconvoluted amide I bands of keratose in solid form, low concentration solution prepared in D_2O and freeze-dried physical hydrogels. Full range of FT-IR spectrum of 2 w/v % keratose solution in D_2O is presented in Figure A.4. Deconvoluted amide I bands of freeze dried chemically crosslinked hydrogels are given in Figure 4.19. Secondary structure content of different forms of keratose are summarized in Table 4.3 and Table 4.4. Unsurprisingly, in its solid form; keratose exhibits a considerably high amount of α-helix sub-structure, with an 86 % composition, as previously supported [73]. However, in the solution form at 2% w/v concentration in D_2O, the negatively charged nature of the protein structure results in an unordered conformation dominantly. As keratose concentration was increased in the solution up to 7.5 or 10% w/v, the content of β-sheet substructures increases. Similar concentration dependence of β-sheet composition was also observed for alanine rich helical proteins [88].

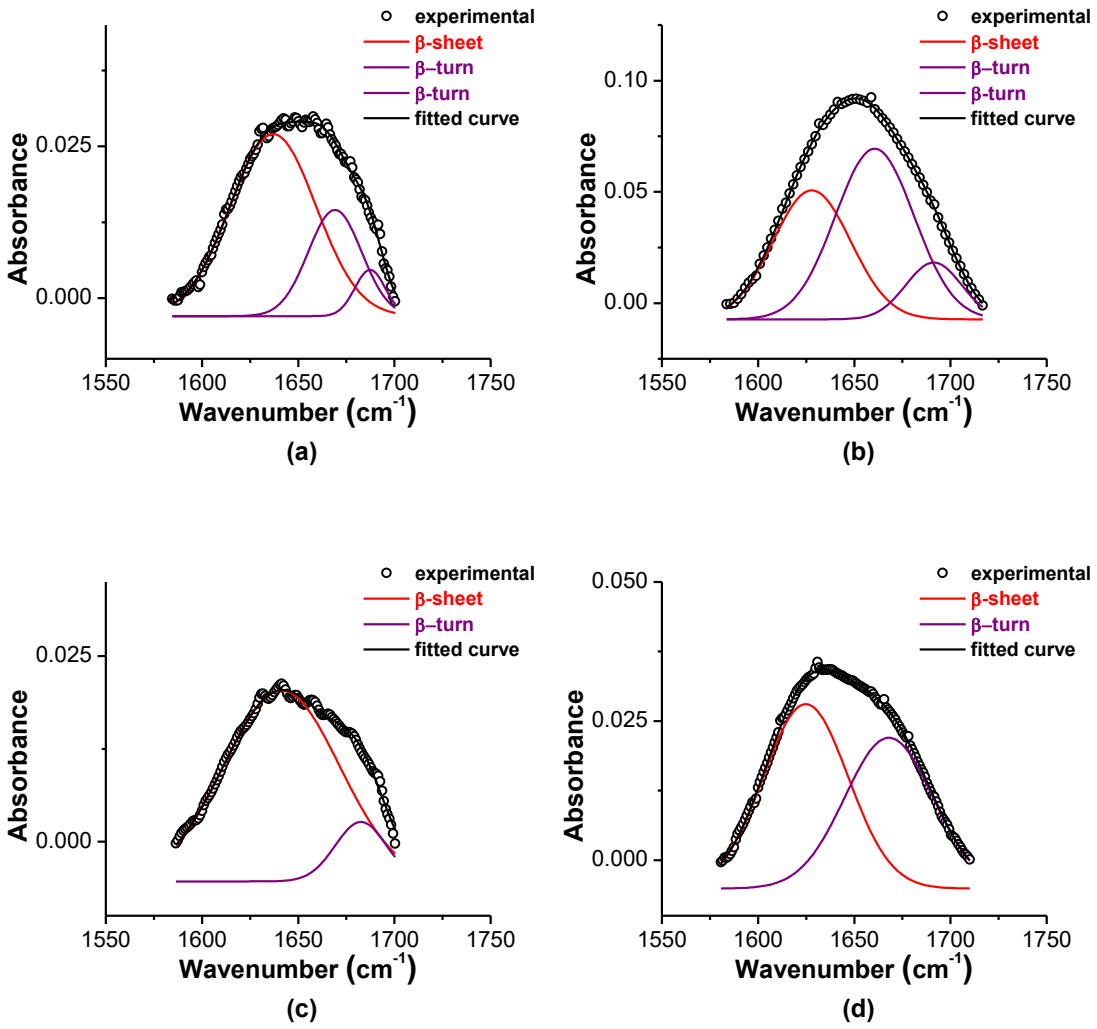

Figure 4.19. Deconvoluted amide I bands of a) 7.5 w/v % keratose solution in D_2O, b) freeze dried 7.5 w/v % keratose hydrogel prepared at 1:1 amine group:crosslinker, c) freeze dried 7.5 w/v % keratose hydrogel prepared at 1:2 amine group:crosslinker, and d) freeze dried 7.5 w/v % keratose hydrogel prepared at 1:4 amine group:crosslinker.

Table 4.3. Secodary structure concents of keratose in solid form, in D_2O and freeze dried physical hydrogel form.

Solid form		**2 w/w % solution in D_2O**		**hydrogel prepared at 37 °C**		**hydrogel prepared at 50 °C**	
band (cm^{-1})	% content	band (cm^{-1})	% content	band (cm^{-1})	% content	band (cm^{-1})	% content
1619	2	1634	60	1633	60	1627	50
1654	86	1648	38	1669	30	1666	40
1691	12	1661	2	1692	10	1692	10

The ordered structures of the chemically crosslinked hydrogels was not seemed to be much affected from the increasing crosslinking density. Even though all three of the chemical hydrogels exhibited high β-sheet content, no significant relation exists between the crosslinker amount and the percent content of molecular conformations (Table 4.2).

Table 4.4. Secodary structure concents of keratose in D_2O and freeze dried chemical hydrogel form.

Uncrosslinked solution		**1:1 crosslinked**		**1:2 crosslinked**		**1:4 crosslinked**	
band (cm^{-1})	% content	band (cm^{-1})	% content	band (cm^{-1})	% content	band (cm^{-1})	% content
1637	69	1628	38	1641	88	1625	54
1669	25	1661	50	1683	12	1668	46
1687	6	1691	12				

CHAPTER 5

CONCLUSION AND FUTURE WORK

Biopolymers have been received increasing attention due to their biocompatible nature and biodegradability making them superior in biomedical applications such as drug delivery and tissue engineering. Among these types of materials, keratin is a highly abundant, well-known protein by being the main constituents of animal parts including hair, feathers, wool, and horn. In this study, characterization and evaluation of self-assembly behavior of keratin-derived proteins were aimed for their possible applications in biomedical area.

Water soluble oxidized form of keratin proteins (or keratoses) were obtained from Akkaraman sheep wool by using peracetic acid treatment with a quite high final yield. AFM observations and DLS measurements suggested that keratose proteins at 5 and 10 mg/ml concentrations in aqueous solutions assembled into globular nanoparticles with diameters of 20-40 nm which makes them suitable for drug delivery applications. On the other hand, at 10% w/v keratose concentration and upon incubation at 37 °C self-assembled interconnected hydrogel network formed with an average pore size of ~ 6 ± 4 μm which is in the proposed range to support fibroblast ingrowth. As assembly temperature was increased from 37 to 50 °C, hydrogel network composed of thicker fibrils with a minimal change in average pore size was obtained. At lower keratose concentration, 7.5% w/v, formation of hydrogels was also triggered by the addition of a crosslinker, THPC. Pore size and morphology of these hydrogels were demonstrated to be tuned by the amount of the crosslinker added.

Oscillatory frequency sweep tests revealed that viscoelastic properties of the keratose hydrogels could easily be controlled by changing hydrogelation parameters such as temperature and amount of the crosslinker. In the preliminary cell culture experiments, select physical hydrogel prepared at 37 °C was observed to support attachment and proliferation of L929 mouse fibroblasts cells as much as collagen films. These results suggested that keratose hydrogels could be promising candidates as scaffolds for soft tissue engineering with tunable viscoelastic and microstructure characteristics.

In future studies, cell proliferation and live/dead assays will be applied to chemical hydrogels as well. Viscoelastic properties of the hydrogels will be investigated in more details by applying time-sweep and creep experiments. Mechanical properties of the hydrogels will further be explored using AFM nanoindentation technique, which enables to determine elastic moduli of hydrogels with a minimal amount of testing points. As a long term objective, injectability and 3D-bioprintability of keratose hydrogels will be evaluated in order to be utilized as reliable sources of biomaterials in tissue engineering as scaffolds and/or in wound healing applications.

REFERENCES

1. Gyurova, Anna Y., Aneta Michna, Ljubomir Nikolov, and Elena Mileva. "Self-assembly of four-and two-antennary oligoglycines in aqueous medium." *Colloids and Surfaces A: Physicochemical and Engineering Aspects* 519 (2017): 106-116.

2. Pugliese, Raffaele, and Fabrizio Gelain. "Peptidic Biomaterials: From Self-Assembling to Regenerative Medicine." *Trends in biotechnology* (2016).

3. Huang, Wenwen, Sreevidhya Krishnaji, Olena Rabotyagova Tokareva, David Kaplan, and Peggy Cebe. "Influence of water on protein transitions: morphology and secondary structure." *Macromolecules* 47, no. 22 (2014): 8107-8114.

4. Ramos, María Luz Peralta, Joaquín Antonio González, Lucas Fabian, Claudio Javier Pérez, María Emilia Villanueva, and Guillermo Javier Copello. "Sustainable and smart keratin hydrogel with pH-sensitive swelling and enhanced mechanical properties." *Materials Science and Engineering: C* 78 (2017): 619-626.

5. Bessa, Paulo C., Raul Machado, Sylvia Nürnberger, Daniela Dopler, Asmita Banerjee, António M. Cunha, J. Carlos Rodríguez-Cabello et al. "Thermoresponsive self-assembled elastin-based nanoparticles for delivery of BMPs." *Journal of Controlled Release* 142, no. 3 (2010): 312-318.

6. Brodin, Jeffrey D., Sarah J. Smith, Jessica R. Carr, and F. Akif Tezcan. "Designed, helical protein nanotubes with variable diameters from a single building block." *Journal of the American Chemical Society* 137, no. 33 (2015): 10468-10471.

7. Lee, Tat, Alan Cooper, Robert P. Apkarian, and Vincent Conticello. "Thermo-reversible self-assembly of nanoparticles derived from elastin-mimetic polypeptides." *Advanced Materials* 12, no. 15 (2000): 1105-1110.

8. Meier, Christoph, and Mark E. Welland. "Wet-spinning of amyloid protein nanofibers into multifunctional high-performance biofibers." *Biomacromolecules* 12, no. 10 (2011): 3453-3459.

9. Miranda, Frederico F., Kenji Iwasaki, Satoko Akashi, Koji Sumitomo, Mime Kobayashi, Ichiro Yamashita, Jeremy RH Tame, and Jonathan G. Heddle. "A self-assembled protein nanotube with high aspect ratio." *Small* 5, no. 18 (2009): 2077-2084.

10. Smeenk, Jurgen M., Peter Schön, Matthijs B. J. Otten, Sylvia Speller, Hendrik G. Stunnenberg, and Jan C. M. van Hest. "Fibril formation by triblock copolymers of silklike β-sheet polypeptides and poly (ethylene glycol)." *Macromolecules* 39, no. 8 (2006): 2989-2997.

11. Wang, Weiping, and Ying Chau. "Self-assembled peptide nanorods as building blocks of fractal patterns." *Soft Matter* 5, no. 24 (2009): 4893-4898.

12. Zhang, Shuguang. "More than just bare scaffolds: towards multi-component and decorated fibrous biomaterials." *Nature Biotechnology* 21 (2003): 1171-1178.

13. Zhou, Qinghan, Juan Lin, Feng Yuan, Zhaoyang Ye, Feng Qiu, Chengkang Tang, Yongzhu Chen, and Xiaojun Zhao. "Self-assembly from low dimension to higher conformation of GGX motif in spider silk protein." *Current Nanoscience* 5, no. 4 (2009): 457-464.

14. Neffe, Axel T., Christian Wischke, Miroslava Racheva, and Andreas Lendlein. "Progress in biopolymer-based biomaterials and their application in controlled drug delivery." *Expert review of medical devices* 10, no. 6 (2013): 813-833.

15. Velema, James, and David Kaplan. "Biopolymer-based biomaterials as scaffolds for tissue engineering." In *Tissue Engineering I*, pp. 187-238. Springer Berlin Heidelberg, 2006.

16. Park, Mira, Hye Kyoung Shin, Byoung-Suhk Kim, Myung Jin Kim, In-Shik Kim, Byung-Yong Park, and Hak-Yong Kim. "Effect of discarded keratin-based biocomposite hydrogels on the wound healing process in vivo." *Materials Science and Engineering: C* 55 (2015): 88-94.

17. Zoccola, Marina, Annalisa Aluigi, and Claudio Tonin. "Characterisation of keratin biomass from butchery and wool industry wastes." *Journal of molecular structure* 938, no. 1 (2009): 35-40.

18. Aluigi, Annalisa, Alessandro Corbellini, Fabio Rombaldoni, Marina Zoccola, and Maurizio Canetti. "Morphological and structural investigation of wool-derived keratin nanofibres crosslinked by thermal treatment." *International journal of biological macromolecules* 57 (2013): 30-37.

19. Zhang, Jing, Yi Li, Jiashen Li, Zheng Zhao, Xuan Liu, Zhi Li, Yanxia Han, Junyan Hu, and Aizheng Chen. "Isolation and characterization of biofunctional keratin particles extracted from wool wastes." *Powder technology* 246 (2013): 356-362.

20. de Guzman, Roche C., and Sina Y. Rabbany. "PEG-Immobilized Keratin for Protein Drug Sequestration and pH-Mediated Delivery." *Journal of drug delivery* 2016 (2016).

21. Li, Qinmei, Lijun Zhu, Ruigang Liu, Da Huang, Xin Jin, Ning Che, Zhuang Li, Xiaozhong Qu, Hongliang Kang, and Yong Huang. "Biological stimuli responsive drug carriers based on keratin for triggerable drug delivery." *Journal of Materials Chemistry* 22, no. 37 (2012): 19964-19973.

22. Ramadoss, Preethi, K. Thanigai Arul, J. Ramana Ramya, M. Rigana Begam, V. Sarath Chandra, and E. Manikandan. "Enhanced mechanical strength and sustained drug release of gelatin/keratin scaffolds." *Materials Letters* 186 (2017): 109-112.

23. Konop, Marek, Dorota Sulejczak, Joanna Czuwara, Piotr Kosson, Aleksandra Misicka, Andrzej W. Lipkowski, and Lidia Rudnicka. "The role of allogenic keratin-derived dressing in wound healing in a mouse model." *Wound Repair and Regeneration* 25, no. 1 (2017): 62-74.

24. Nayak, Kush Kumar, and Pratima Gupta. "Study of the keratin-based therapeutic dermal patches for the delivery of bioactive molecules for wound treatment." *Materials Science and Engineering: C* 77 (2017): 1088-1097.

25. Wang, Ju, Shilei Hao, Tiantian Luo, Tao Zhou, Xin Yang, and Bochu Wang. "Keratose/poly (vinyl alcohol) blended nanofibers: Fabrication and biocompatibility assessment." *Materials Science and Engineering: C* 72 (2017): 212-219.

26. Li, Jia-Shen, Yi Li, Xuan Liu, Jing Zhang, and Yu Zhang. "Strategy to introduce an hydroxyapatite–keratin nanocomposite into a fibrous membrane for bone tissue engineering." *Journal of Materials Chemistry B* 1, no. 4 (2013): 432-437.

27. Saravanan, S., D. K. Sameera, A. Moorthi, and N. Selvamurugan. "Chitosan scaffolds containing chicken feather keratin nanoparticles for bone tissue engineering." *International journal of biological macromolecules* 62 (2013): 481-486.

28. Zhang, Hualin, and Jinsong Liu. "Electrospun poly (lactic-co-glycolic acid)/wool keratin fibrous composite scaffolds potential for bone tissue engineering applications." *Journal of Bioactive and Compatible Polymers* 28, no. 2 (2013): 141-153.

29. Tachibana, Akira, Yasunari Furuta, Hideyuki Takeshima, Toshizumi Tanabe, and Kiyoshi Yamauchi. "Fabrication of wool keratin sponge scaffolds for long-term cell cultivation." *Journal of Biotechnology* 93, no. 2 (2002): 165-170.

30. Sando, Lillian, Misook Kim, Michelle L. Colgrave, John AM Ramshaw, Jerome A. Werkmeister, and Christopher M. Elvin. "Photochemical crosslinking of soluble wool keratins produces a mechanically stable biomaterial that supports cell adhesion and proliferation." *Journal of Biomedical Materials Research Part A* 95, no. 3 (2010): 901-911.

31. Yamauchi, Kiyoshi, Masashi Maniwa, and Takeshi Mori. "Cultivation of fibroblast cells on keratin-coated substrata." *Journal of Biomaterials Science, Polymer Edition* 9, no. 3 (1998): 259-270.

32. Sierpinski, Paulina, Jeffrey Garrett, Jianjun Ma, Peter Apel, David Klorig, Thomas Smith, L. Andrew Koman, Anthony Atala, and Mark Van Dyke. "The use of keratin biomaterials derived from human hair for the promotion of rapid regeneration of peripheral nerves." *Biomaterials* 29, no. 1 (2008): 118-128.

33. Vu, Trang, Ye Xue, Trinh Vuong, Matthew Erbe, Christopher Bennet, Ben Palazzo, Lucas Popielski, Nelson Rodriguez, and Xiao Hu. "Comparative Study of Ultrasonication-Induced and Naturally Self-Assembled Silk Fibroin-Wool Keratin Hydrogel Biomaterials." *International Journal of Molecular Sciences* 17, no. 9 (2016): 1497.

34. Sri, Bindu, V. Ashok, and C. Arkendu. "As a review on hydrogels as drug delivery in the pharmaceutical field." *Int J Pharm Chem Sci* 1, no. 2 (2012): 642-61.

35. Guvendiren, Murat, Hoang D. Lu, and Jason A. Burdick. "Shear-thinning hydrogels for biomedical applications." *Soft Matter* 8, no. 2 (2012): 260-272.

36. Ganji, Fariba, and Ebrahim Vasheghani-Farahani. "Hydrogels in controlled drug delivery systems." *Iranian Polymer Journal* 18, no. 1 (2009): 63-88.

37. Patel, Alpesh, and Kibret Mequanint. "Hydrogel biomaterials." In *Biomedical engineering-frontiers and challenges*. InTech, 2011.

38. Hoffman, Allan S. "Hydrogels for biomedical applications." *Advanced drug delivery reviews* 64 (2012): 18-23.

39. Lowman, Anthony M., and Nikolaos A. Peppas. "Hydrogels." *Encyclopedia of controlled drug delivery* 1 (1999): 397-418.

40. Sionkowska, Alina. "Current research on the blends of natural and synthetic polymers as new biomaterials: Review." *Progress in Polymer Science* 36, no. 9 (2011): 1254-1276.

41. Silva, Nuno H. C. S., Carla Vilela, Isabel M. Marrucho, Carmen S. R. Freire, Carlos Pascoal Neto, and Armando J. D. Silvestre. "Protein-based materials: from sources to innovative sustainable materials for biomedical applications." *Journal of Materials Chemistry B* 2, no. 24 (2014): 3715-3740.

42. Li, Yanmei, Yanfang Wang, Jingjie Ye, Jiang Yuan, and Yinghong Xiao. "Fabrication of poly (ε-caprolactone)/keratin nanofibrous mats as a potential scaffold for vascular tissue engineering." *Materials Science and Engineering: C* 68 (2016): 177-183.

43. Devine, Declan M., and Clement L. Higginbotham. "The synthesis of a physically crosslinked NVP based hydrogel." *Polymer* 44, no. 26 (2003): 7851-7860.

44. Sri, Bindu, Ashok Vadithya, and Arkendu Chatterjee. "As a review on hydrogels as drug delivery in the pharmaceutical field." *International Journal of Pharmaceutical and Chemical Sciences* 1, no. 2 (2012): 642-61.

45. Wang, Bin, Wen Yang, Joanna McKittrick, and Marc André Meyers. "Keratin: Structure, mechanical properties, occurrence in biological organisms, and efforts at bioinspiration." *Progress in Materials Science* 76 (2016): 229-318.

46. Richter, Jillian R., Roche C. de Guzman, Olga K. Greengauz-Roberts, and Mark Van Dyke. "Structure–property relationships of meta-kerateine biomaterials derived from human hair." *Acta biomaterialia* 8, no. 1 (2012): 274-281.

47. Ruan, Jishou, Kui Wang, Jie Yang, Lukasz A. Kurgan, and Krzysztof Cios. "Highly accurate and consistent method for prediction of helix and strand content from primary protein sequences." *Artificial Intelligence in Medicine* 35, no. 1 (2005): 19-35.

48. Cheng, Haitao, Taner Z. Sen, Andrzej Kloczkowski, Dimitris Margaritis, and Robert L. Jernigan. "Prediction of protein secondary structure by mining structural fragment database." *Polymer* 46, no. 12 (2005): 4314-4321.

49. Rouse, Jillian G., and Mark E. Van Dyke. "A review of keratin-based biomaterials for biomedical applications." *Materials* 3, no. 2 (2010): 999-1014.

50. Cardamone, Jeanette M. "Investigating the microstructure of keratin extracted from wool: Peptide sequence (MALDI-TOF/TOF) and protein conformation (FTIR)." *Journal of molecular structure* 969, no. 1 (2010): 97-105.

51. Atav, Riza. "Thermodynamics of wool dyeing." In *Thermodynamics Fundamentals and Its Application in Science*. InTech, 2012.

52. de Guzman, Roche C., Michelle R. Merrill, Jillian R. Richter, Rawad I. Hamzi, Olga K. Greengauz-Roberts, and Mark E. Van Dyke. "Mechanical and biological properties of keratose biomaterials." *Biomaterials* 32, no. 32 (2011): 8205-8217.

53. Jain, Aditi, Venkatraman Ravi, Jaseer Muhamed, Kaushik Chatterjee, and Nagalingam R. Sundaresan. "A simplified protocol for culture of murine neonatal cardiomyocytes on nanoscale keratin coated surfaces." *International journal of cardiology* 232 (2017): 160-170.

54. Ferroni, Claudia, Giovanna Sotgiu, Anna Sagnella, Greta Varchi, Andrea Guerrini, Demetra Giuri, Eleonora Polo et al. "Wool keratin 3D scaffolds with light-triggered antimicrobial activity." *Biomacromolecules* 17, no. 9 (2016): 2882-2890.

55. Ham, Trevor R., Ryan T. Lee, Sangheon Han, Salma Haque, Yael Vodovotz, Junnan Gu, Luke R. Burnett, Seth Tomblyn, and Justin M. Saul. "Tunable keratin hydrogels for controlled erosion and growth factor delivery." *Biomacromolecules* 17, no. 1 (2015): 225-236.

56. Ferraro, Vincenza, Marc Anton, and Véronique Santé-Lhoutellier. "The “sisters” α-helices of collagen, elastin and keratin recovered from animal by-products: Functionality, bioactivity and trends of application." *Trends in Food Science & Technology* 51 (2016): 65-75.

57. Jin, Xingxing, Yanfang Wang, Jiang Yuan, and Jian Shen. "Extraction, characterization, and NO release potential of keratin from human hair." *Materials Letters* 175 (2016): 188-190.

58. Van Dyke, Mark E., and Thaleia Teli. "Keratin compositions for treatment of bone deficiency or injury." U.S. Patent 9,220,754, issued December 29, 2015.

59. Tanabe, Toshizumi, Naoya Okitsu, and Kiyoshi Yamauchi. "Fabrication and characterization of chemically crosslinked keratin films." *Materials Science and Engineering: C* 24, no. 3 (2004): 441-446.

60. Ratner, Buddy D., Thomas Horbett, Allan S. Hoffman, and Stephen D. Hauschka. "Cell adhesion to polymeric materials: implications with respect to biocompatibility." *Journal of biomedical materials research* 9, no. 5 (1975): 407-422.

61. Reichl, Stephan. "Films based on human hair keratin as substrates for cell culture and tissue engineering." *Biomaterials* 30, no. 36 (2009): 6854-6866.

62. Wang, Ju, Shilei Hao, Tiantian Luo, Zhongjun Cheng, Wenfeng Li, Feiyan Gao, Tingwang Guo, Yuhua Gong, and Bochu Wang. "Feather keratin hydrogel for wound repair: Preparation, healing effect and biocompatibility evaluation." *Colloids and Surfaces B: Biointerfaces* 149 (2017): 341-350.

63. Cruz, Célia F., Nuno G. Azoia, Teresa Matamá, and Artur Cavaco-Paulo. "Peptide—protein interactions within human hair keratins." *International Journal of Biological Macromolecules* 101 (2017): 805-814.

64. Han, Sangheon, Trevor R. Ham, Salma Haque, Jessica L. Sparks, and Justin M. Saul. "Alkylation of human hair keratin for tunable hydrogel erosion and drug delivery in tissue engineering applications." *Acta biomaterialia* 23 (2015): 201-213.

65. Turner, Emily, Luke Burnett, and Saami K. Yazdani. "Keratose as a Novel Drug Carrier for Drug Coated Balloons." In *Biomedical Engineering Conference (SBEC), 2016 32nd Southern*, pp. 71-72. IEEE, 2016.

66. Ki, Chang Seok, Eun Hee Gang, In Chul Um, and Young Hwan Park. "Nanofibrous membrane of wool keratose/silk fibroin blend for heavy metal ion adsorption." *Journal of Membrane Science* 302, no. 1 (2007): 20-26.

67. Yalçın, Hakan, and Mehmet Ali Kaya. "Anadolu yaban koyunu ve akkaraman koyununun kafa kemikleri üzerinde karşılaştırmalı geometrik morfometri." *Atatürk Üniversitesi Veteriner Bilimleri Dergisi* 4, no. 2 (2009).

68. Schneider, Caroline A., Wayne S. Rasband, and Kevin W. Eliceiri. "NIH Image to ImageJ: 25 years of image analysis." *Nature methods* 9, no. 7 (2012): 671-675.

69. Kong, Jilie, and Shaoning Yu. "Fourier transform infrared spectroscopic analysis of protein secondary structures." *Acta biochimica et biophysica Sinica* 39, no. 8 (2007): 549-559.

70. Hilterhaus-Bong, Sabine, and Helmut Zahn. "Contributions to the chemistry of human hair. 1. Analyses of cystine, cysteine and cystine oxides in untreated human hair." *International journal of cosmetic science* 9, no. 3 (1987): 101-110.

71. Cardamone, Jeanette M., Alberto Nuñ, Rafael A. Garcia, and Mila Aldema-Ramos. "Characterizing wool keratin." *Advances in Materials Science and Engineering* 2009 (2009).

72. Eslahi, Niloofar, Fatemeh Dadashian, and Nahid Hemmati Nejad. "An investigation on keratin extraction from wool and feather waste by enzymatic hydrolysis." *Preparative Biochemistry and Biotechnology* 43, no. 7 (2013): 624-648.

73. Kakkar, Prachi, and Balaraman Madhan. "Fabrication of keratin-silica hydrogel for biomedical applications." *Materials Science and Engineering: C* 66 (2016): 178-184.

74. Xie, Haibo, Shenghai Li, and Suobo Zhang. "Ionic liquids as novel solvents for the dissolution and blending of wool keratin fibers." *Green Chemistry* 7, no. 8 (2005): 606-608.

75. Wang, Kui, Rong Li, Jihong Ma, Yingkai Jian, and Jiangning Che. "Extracting keratin from wool by using L-cysteine." *Green Chemistry* 18, no. 2 (2016): 476-481.

76. Darapuneni, Rama Rao and Bhuvanesh Gupta. "Crystallite orientation in wool fibers." *Journal of applied polymer science* 46, no. 6 (1992): 1109-1112.

77. Kanzaki, Noriko, Taro Q. P. Uyeda, and Kazuo Onuma. "Intermolecular interaction of actin revealed by a dynamic light scattering technique." *The Journal of Physical Chemistry B* 110, no. 6 (2006): 2881-2887.

78. Armstrong, Jonathan K., Rosalinda B. Wenby, Herbert J. Meiselman, and Timothy C. Fisher. "The hydrodynamic radii of macromolecules and their effect on red blood cell aggregation." *Biophysical journal* 87, no. 6 (2004): 4259-4270.

79. Lu, Zhiming, Fang Pan, Dong Wang, Mario Campana, Hai Xu, Ian M. Tucker, Jordan T. Petkov, John Webster, and Jian R. Lu. "Unusual surface and solution behaviour of keratin polypeptides." *RSC Advances* 6, no. 107 (2016): 105192-105201.

80. Annabi, Nasim, Jason W. Nichol, Xia Zhong, Chengdong Ji, Sandeep Koshy, Ali Khademhosseini, and Fariba Dehghani. "Controlling the porosity and microarchitecture of hydrogels for tissue engineering." *Tissue Engineering Part B: Reviews* 16, no. 4 (2010): 371-383.

81. Jang, Jinhyeong, Jisu Hong, and Chaenyung Cha. "Effects of precursor composition and mode of crosslinking on mechanical properties of graphene oxide reinforced composite hydrogels." *Journal of the Mechanical Behavior of Biomedical Materials* 69 (2017): 282-293.

82. Cho, Jaepyoung, Marie-Claude Heuzey, André Bégin, and Pierre J. Carreau. "Physical gelation of chitosan in the presence of β-glycerophosphate: the effect of temperature." *Biomacromolecules* 6, no. 6 (2005): 3267-3275.

83. Ozbas, Bulent, Juliana Kretsinger, Karthikan Rajagopal, Joel P. Schneider, and Darrin J. Pochan. "Salt-triggered peptide folding and consequent self-assembly into hydrogels with tunable modulus." *Macromolecules* 37, no. 19 (2004): 7331-7337.

84. Wang, Shuai, Francesca Taraballi, Lay Poh Tan, and Kee Woei Ng. "Human keratin hydrogels support fibroblast attachment and proliferation in vitro." *Cell and tissue research* 347, no. 3 (2012): 795-802.

85. Chung, Cindy, Kyle J. Lampe, and Sarah C. Heilshorn. "Tetrakis (hydroxymethyl) phosphonium chloride as a covalent cross-linking agent for cell encapsulation within protein-based hydrogels." *Biomacromolecules* 13, no. 12 (2012): 3912-3916.

86. Rammensee, S., D. Huemmerich, K. D. Hermanson, T. Scheibel, and A. R. Bausch. "Rheological characterization of hydrogels formed by recombinantly produced spider silk." *Applied Physics A* 82, no. 2 (2006): 261.

87. Xing, Qi, Keegan Yates, Caleb Vogt, Zichen Qian, Megan C. Frost, and Feng Zhao. "Increasing mechanical strength of gelatin hydrogels by divalent metal ion removal." *Scientific reports* 4 (2014).

88. Farmer, Robin S., Lindsey M. Argust, Jared D. Sharp, and Kristi L. Kiick. "Conformational properties of helical protein polymers with varying densities of chemically reactive groups." *Macromolecules* 39, no. 1 (2006): 162-170.

APPENDIX A

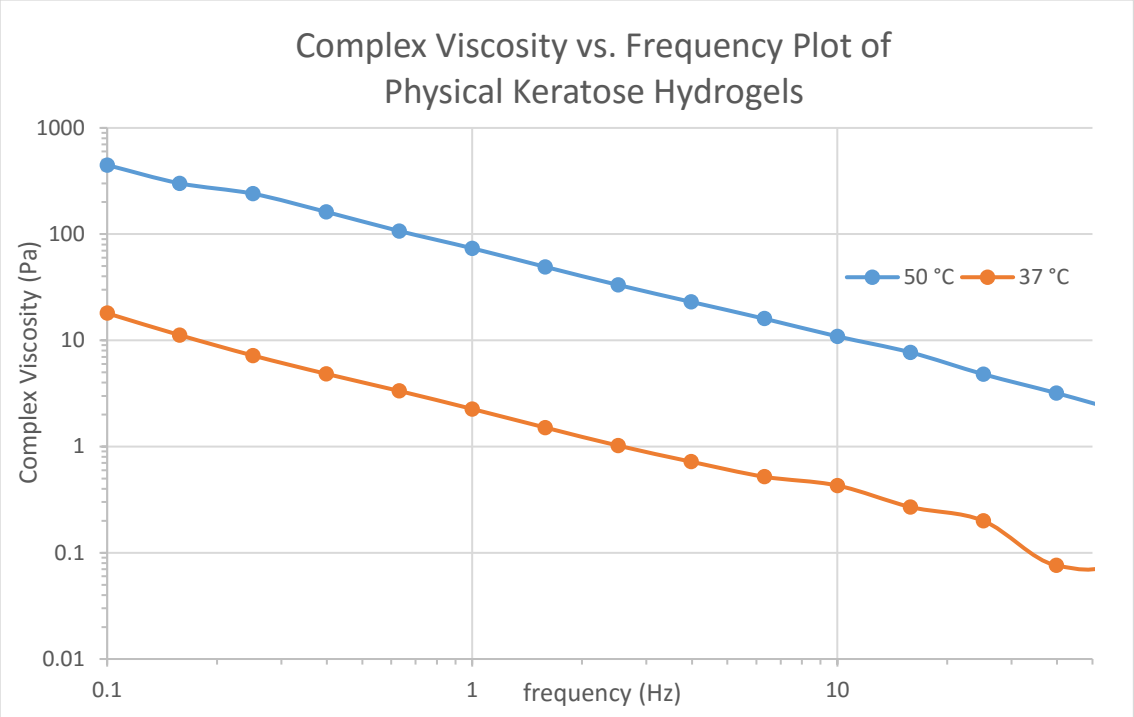

Figure A.1. Complex viscosity vs. frequency plot of self-assembled keratose hydrogels.

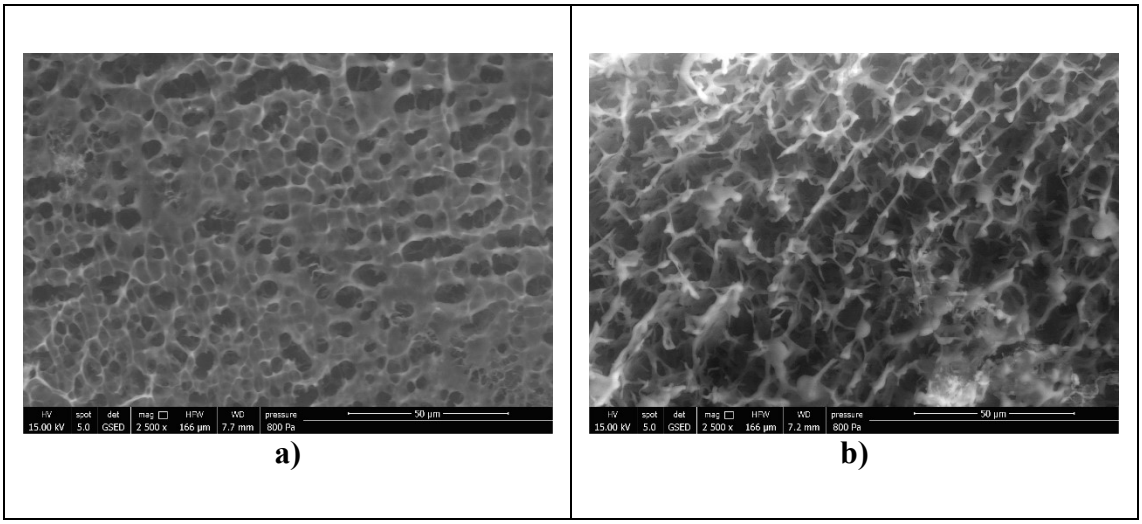

Figure A.2. SEM pictures of freeze-dried physical keratose hydrogels prepared at a) 37 °C, b) 50 °C, top view; scale bar = 50 µm.

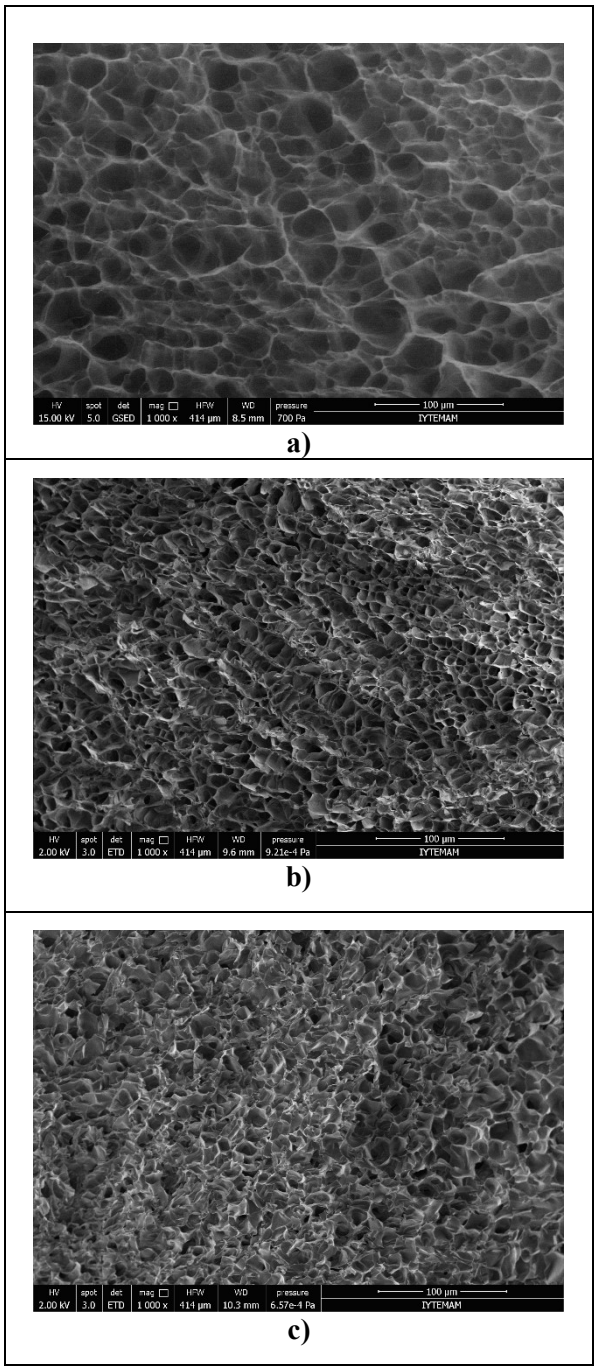

Figure A.3. SEM pictures of freeze-dried chemical keratose hydrogels prepared at amine group:crosslinker ratios; a) 1:1, b) 1:2, and c) 1:4, top view; scale bar = 100 µm.

Table A.1. p-values of cell culture supporting medium pairs at incubation days 1 and 5

Pair	p-values	
	Day 1	Day 5
Blank TCPS-collagen	0.048	0.886
Blank TCPS-keratose hydrogel	0.048	0.96
Collagen-keratose hydrogel	0.844	0.888

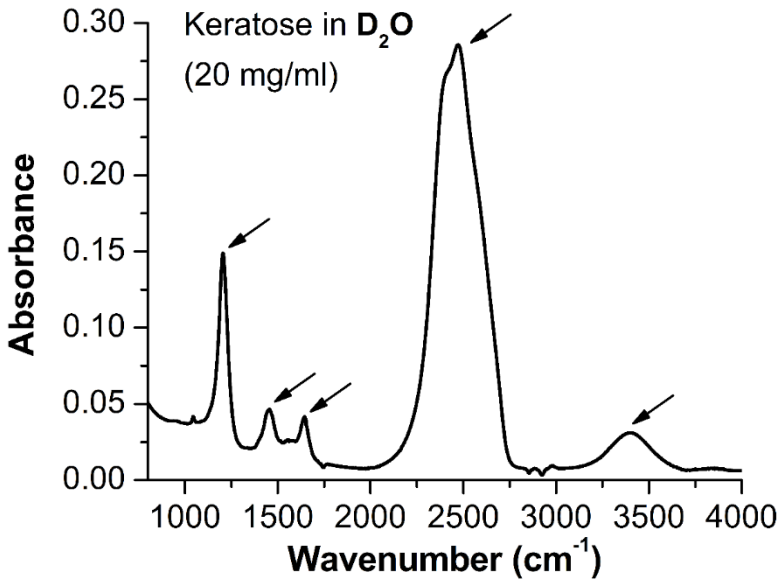

Figure A.4. FT-IR spectrum of 2 w/v % keratose solution in D_2O, drawn in a scale of wavenumbers 800-4000 cm^{-1}.